DALTON
FULL PAPER

Electronic and magnetic metal–metal interactions in dinuclear oxomolybdenum(V) complexes across bis-phenolate bridging ligands with different spacers between the phenolate termini: ligand-centred *vs.* metal-centred redox activity

Simon R. Bayly,[a] Elizabeth R. Humphrey,[a] Helena de Chair,[a] Cecilia G. Paredes,[a] Zoe R. Bell,[a] John C. Jeffery,[a] Jon A. McCleverty,*[a] Michael D. Ward,*[a] Federico Totti,[b] Dante Gatteschi,[b] Stephane Courric,[c] Barry R. Steele[c] and Constantinos G. Screttas[c]

[a] *School of Chemistry, University of Bristol, Cantock's Close, Bristol, UK BS8 1TS. E-mail: mike.ward@bristol.ac.uk*
[b] *Department of Chemistry, University of Florence, Via Maragliano 75/77, 50144 Florence, Italy*
[c] *Institute of Organic and Pharmaceutical Chemistry, National Hellenic Research Foundation, 48 Vas. Constantinou Ave., 116 35 Athens, Greece*

Received 18th January 2001, Accepted 22nd March 2001
First published as an Advance Article on the web 17th April 2001

A series of dinuclear complexes has been prepared in which two {$Mo^{V}(Tp^{Me,Me})(O)Cl$} fragments (abbreviated as **Mo**; $Tp^{Me,Me}$ = tris(3,5-dimethylpyrazol-1-yl)hydroborate) are attached to either end of a bis-*p*-phenolate bridging ligand $[(4,4'\text{-}OC_6H_4)\text{–}X\text{–}(4,4'\text{-}C_6H_4O)]^{2-}$. The complexes are **$Mo_2(C{=}C)$** (X = CH=CH), **$Mo_2(C{=}C)_2$** (X = CH=CH–CH=CH), **$Mo_2(C{=}C)_3$** (X = CH=CH–CH=CH–CH=CH), **$Mo_2(th)$** (X = 2,5-thiophenediyl), **$Mo_2(th)_2$** (X = 2,5:2′,5′-bithiophenediyl), **$Mo_2(th)_3$** (X = 2,5:2′,5′:2″,5″-terthiophenediyl), **$Mo_2(C{\equiv}C)$** (X = C≡C), **$Mo_2(N{=}N)$** (X = N=N), **$Mo_2(CO)$** [X = C(O)] and **$Mo_2(C_2\Phi C_2)$** [X = CH=CH(1,4-C_6H_4)CH=CH]. Electrochemical, UV/VIS/NIR spectroelectrochemical and magnetic measurements have been carried out in order to see how effectively the different spacer groups X mediate electronic and magnetic interactions between the two redox-active, paramagnetic, **Mo** centres. The electronic interactions were determined from the redox separation between the two successive one-electron oxidations which are formally Mo(VI)–Mo(V) couples; it was found that thienyl units in the bridging ligand are much more effective at maintaining electronic communication over long distances than *p*-phenylene or ethenyl spacers of comparable lengths. The azo (N=N) linkage afforded a much weaker electronic interaction than the ethenyl or ethynyl spacers. UV/VIS/NIR spectroelectrochemical studies showed that whereas the first oxidation is metal-centred to give Mo(VI)–Mo(V) species with characteristic intense phenolate→Mo(VI) LMCT transitions in the near-IR region, the spectra of the doubly oxidised complexes are characteristic of quinones: thus, the sequence of species formed on oxidation is $[Mo(V)(\mu\text{-diolate})Mo(V)]^{0} \longrightarrow [Mo(V)(\mu\text{-diolate})Mo(VI)]^{+} \longrightarrow [Mo(V)(\mu\text{-quinone})Mo(V)]^{2+}$, with an internal charge redistribution associated with the second oxidation. Semi-empirical ZINDO calculations provide some support for this. Magnetic susceptibility measurements on **$Mo_2(C{=}C)$**, **$Mo_2(th)$**, **$Mo_2(N{=}N)$** and **$Mo_2(C{\equiv}C)$** show that all are weakly antiferromagnetically coupled, as expected on the basis of a spin-polarisation picture, with the order of strength of the magnetic interaction being the reverse of the order for electronic coupling, such that **$Mo_2(th)$** affords the strongest electronic interaction but the weakest magnetic interaction.

Introduction

We have been interested recently in examining how magnetic and electronic interactions between metal centres in polynuclear complexes are controlled by the nature of the bridging ligand which links them.[1–9] Electronic interactions between redox-active metal fragments, as manifested by a separation between metal-centred redox couples and the consequent formation of stable mixed-valence states, have been of interest since the discovery of the Creutz–Taube ion; subsequently, long-range electron-transfer in mixed-valence complexes has been extensively studied because of its relevance to the preparation of 'molecular wires' which might permit charge transport in nanoscopic circuits.[10–14] The effects of length, substitution pattern (*i.e. para vs. meta*), and conformation of the bridging ligand on the extent of the electronic metal–metal interactions have all been studied in some detail. We[2,4–7] and others[15] have recently been interested to see how these properties of the bridging ligand also control the *magnetic* metal–metal interaction.

It has generally been the case that magnetic and electronic interactions are treated quite separately, despite the fact that both clearly depend on the nature of the bridging ligand through which the interaction is transmitted (as long as the metal centres are far enough apart that direct metal–metal orbital overlap can be excluded). This reflects the fact that the complexes most commonly used to probe electronic interactions are based on kinetically inert, diamagnetic metal fragments such as Ru(II),[10–14] whereas studies on magnetic exchange interactions commonly involve labile metals such as first-row transition-metal and lanthanide(III) ions in coordination environments where they do not show reversible redox interconversions.[16–23] In our recent work we have performed *combined* studies of electronic and magnetic interactions in

dinuclear complexes $\mathbf{Mo_2}(OO)$,[2,3,5,6,8] using the $\{Mo^{V}(Tp^{Me,Me})(O)Cl\}$ fragment (first described by Enemark and co-workers,[24] and abbreviated **Mo**; $Tp^{Me,Me}$ = tris(3,5-dimethylpyrazol-1-yl)hydroborate) attached to either end of a bis-phenolate bridging ligand (denoted *OO*). This metal fragment is paramagnetic (d^1 configuration), which has allowed study of magnetic exchange as a function of the bridging ligand, and we have shown that the sign of the magnetic exchange interaction can be predicted according to the number of atoms in the bridging pathway, according to a simple spin-polarisation picture.[1,2,4–7] The **Mo** fragment is also redox-active, with reversible Mo(V)–Mo(IV) and Mo(VI)–Mo(V) couples, such that electronic interactions can also be studied by measurements of redox separations in cyclic voltammograms and by spectroscopic studies on the Mo(V)–Mo(IV) and Mo(VI)–Mo(V) mixed-valence states.[2,3,8] Although magnetic exchange and electronic delocalisation are quite different phenomena, it has become apparent that there are strong correlations between them because of their shared dependence on the structure of the bridging ligand.[2]

In addition to their electrochemical and magnetic properties, the dinuclear complexes $[\{Mo^{V}(Tp^{Me,Me})(O)Cl\}_2(\mu\text{-}OO)]$ have also proved to be of interest for their optical spectroscopic properties in the oxidised Mo(VI)–Mo(V) and Mo(VI)–Mo(VI) forms.[3,25,26] On oxidation of a molybdenum(V) centre to the molybdenum(VI) state, the phenolate→Mo(V) LMCT transition in the visible region is replaced by a much more intense transition which, in many of the dinuclear complexes, lies in the near-infrared region (900–1400 nm) and has been assigned as phenolate→Mo(VI) LMCT.[3] Thus the complexes act as electrochromic dyes which can be switched, by a simple reversible redox process, between transparent and essentially opaque states in a region of the spectrum which is of interest for telecommunications and optical data processing. We have accordingly been exploiting this property of some of these complexes in optical materials-related applications.[26]

In this paper we describe the syntheses, electrochemical, spectroscopic and spectroelectrochemical, and magnetic properties of further complexes of this type (see Scheme 1 for the structures of the bridging ligands and their abbreviations): specifically, a series of complexes based on *para*-substituted bis-phenolate ligands with a variety of different spacer groups separating the two phenolate termini. The ligands H_2**th**, H_2(**th**)$_2$ and H_2(**th**)$_3$ contain one, two or three 2,5-thienyl spacers respectively. We were interested in these because oligothiophene chains are known to be particularly effective at mediating long-distance electronic interactions because of their favourable steric and electronic properties.[27–30] They are more likely to be coplanar than oligophenylene chains because the steric interaction between the H^3/H^4 protons of adjacent thienyl rings is less than that between the H^2/H^6 protons of adjacent C_6H_4 units; this leads to more effective delocalisation, which is further enhanced by the participation of π-symmetry S orbitals in the conjugated system. The ligands H_2(**C=C**), H_2(**C=C**)$_2$ and H_2(**C=C**)$_3$ were likewise prepared to examine how electronic interactions in this series of complexes are attenuated by double bond spacers; H_2(**C$_2$ΦC$_2$**) is even longer than H_2(**C=C**)$_3$, having (effectively) four double bonds between the phenolate termini, counting one phenylene spacer as comparable to two double bonds in the bridging pathway. Ligands H_2(**C≡C**) (alkynyl linkage) and H_2(**NN**) (azo linkage) are two-atom conjugated spacers to compare with H_2(**C=C**). In contrast to these, 4,4′-dihydroxybenzophenone (H_2**CO**) contains only one additional atom in the direct conjugated pathway between the two phenol termini.

The aims of this work have been: (i) to compare and contrast the abilities of these different spacer units to mediate electronic and magnetic interactions; (ii) to evaluate by spectroelectrochemical methods the spectroscopic properties of the complexes in all accessible oxidation states, to see which are most effective as potential electrochromic dyes for use in the NIR region; and (iii) to address fundamental questions of metal-centred *vs.* ligand-centred redox activity in complexes where the bridging ligand is non-innocent.

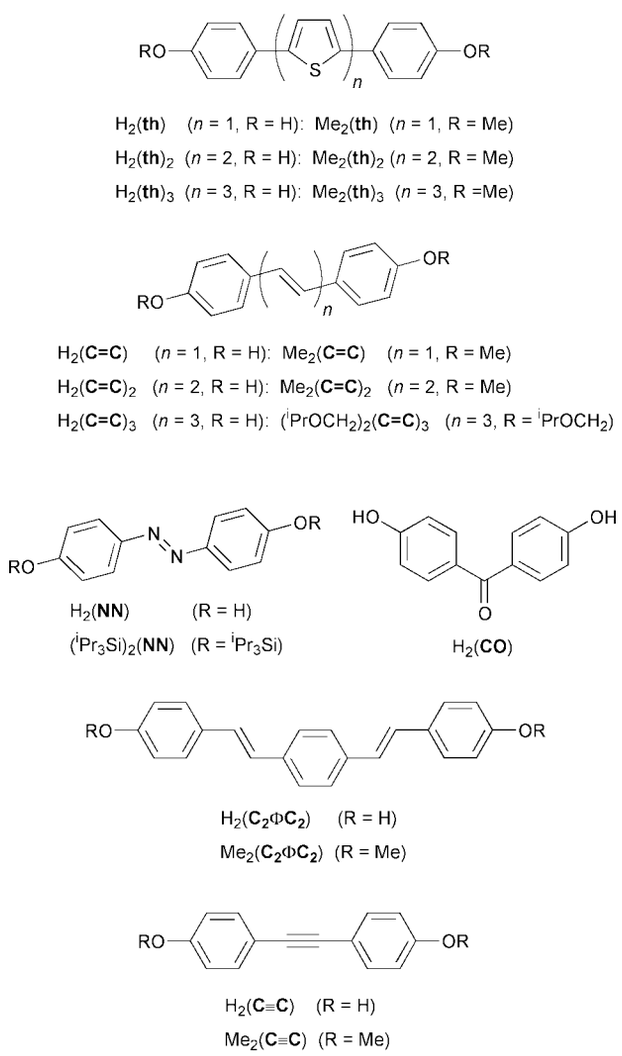

Scheme 1 Structural formulae of the bridging ligands used in this paper and their protected precursors.

Results and discussion

Syntheses of ligands

The synthesis of H_2**th** has been reported by Takahashi *et al.*, and involved addition of the aromatic groups to the thienyl core in two separate metallation/cross-coupling stages. Pd-catalysed coupling of 2-thienylzinc chloride with 4-iodoanisole afforded 2-(4-methoxyphenyl)thiophene; remetallation of the thienyl unit with zinc chloride, and a second cross-coupling with 4-iodoanisole, afforded 2,5-bis(4-methoxyphenyl)thiophene which was demethylated using BBr_3 to give H_2**th**.[31] We have developed a more convenient synthesis based on Pd-catalysed coupling of both phenyl substituents simultaneously to 2,5-bis-(tri-n-butylstannyl)thiophene, to give the protected 2,5-bis(4-methoxyphenyl)thiophene which was demethylated using molten pyridinium chloride. We have previously described the preparation of H_2(**th**)$_2$ from 5,5″-bis(tri-n-butylstannyl)-2,2′-bithiophene using this method,[27] and it is also effective for preparation of H_2(**th**)$_3$ starting from 5,5″-bis(tri-n-butylstannyl)-2,2′:5′,2″-terthiophene.

The ethenyl-bridged ligand H_2(**C=C**) was simply prepared by a Heck coupling of 4-vinylanisole with 4-bromoanisole to give 1,2-bis(4-methoxyphenyl)stilbene, followed by demethylation

Table 1 Analytical and mass spectroscopic data for the new complexes

Complex[a]	Yield (%)	Analysis (%)[b] C	H	N	M^+ by FAB MS *m/z*
Mo_2(th)	60	48.1 (47.8)	4.9 (4.7)	14.9 (14.6)	1155
Mo_2(th)$_2$	59	49.9 (50.7)	5.1 (5.3)	12.6 (12.7)	1237
Mo_2(th)$_3$	35	48.4 (48.6)	4.9 (4.8)	12.6 (12.2)[c]	1319
Mo_2(C=C)	15	49.1 (49.3)	4.9 (5.3)	14.5 (14.7)[d]	1100
Mo_2(C=C)$_2$	56	47.9 (47.8)	4.8 (4.9)	13.9 (14.4)[e]	1127
Mo_2(C=C)$_3$	39	47.6 (47.6)	5.2 (4.9)	13.0 (13.6)[f]	1152
Mo_2(C≡C)	37	47.3 (47.3)	5.3 (5.4)	13.5 (13.5)[g]	1098
Mo_2(N=N)	30	46.6 (47.2)	5.2 (5.2)	16.6 (17.1)[d]	1103
Mo_2(CO)	65	44.5 (44.5)	5.0 (4.6)	13.8 (14.2)[f]	1102
Mo_2(C_2PhC_2)	8	[h]			1202

[a] All complexes are dark green, apart from **Mo_2(N=N)** which is brown and **Mo_2(CO)** which is maroon. [b] Expected values in parentheses. [c] 2 MeOH in elemental analysis. [d] 0.5 hexane in elemental analysis. [e] 0.5 CH_2Cl_2 in elemental analysis. [f] 1 CH_2Cl_2 in elemental analysis. [g] 3 MeOH in elemental analysis. [h] We could not obtain reliable and repeatable analytical data for this complex.

with BBr_3; this is a considerable improvement on the published procedure which is nearly 40 years old.[32] The syntheses of H_2(**C=C**)$_2$ and H_2(**C=C**)$_3$ (as their protected precursors) are based on published methods,[33,34] although the use of the n-propyloxy methyl ether protecting group in the synthesis of H_2(**C=C**)$_3$ is new. The protected (MeO protecting groups) precursor of H_2(**C=C**)$_2$ was then demethylated by reaction with MeMgBr, following the method of Takahashi *et al.*[35] Attempts to use more traditional deprotecting reagents such as BBr_3 or pyridine hydrochloride were in our hands much less successful, giving mixtures of products which included (according to mass spectroscopy of the crude products) a dimer of the deprotected ligand, possibly arising from a Lewis-acid induced Diels–Alder reaction.[36] Given the evident fragility of the polyene chain of H_2(**C=C**)$_2$ under the rather harsh conditions used for demethylating the methyl ether group, the acetal-based n-propyloxy methyl ether protecting group[37] was used for the synthesis of H_2(**C=C**)$_3$, as it could be removed under mild conditions (HCl in MeOH–thf).

The ethynyl-bridged ligand H_2(**C≡C**) has also been reported before,[38,39] although the syntheses are again capable of improvement in the light of more recent techniques. We prepared 1,2-bis(4-methoxyphenyl)ethyne by a modification of the Sonogashira–Hagihara coupling of acetylene gas with aryl halides,[40] in which 2-methyl-3-butyn-2-ol, a protected form of acetylene, is used instead of acetylene gas.[41] This necessitates addition of a base to the reaction mixture in order to remove the protecting group *in situ*, and we used a heterogeneous base (KOH) in conjunction with a phase-transfer agent in order to maintain a constant but low concentration of base in the organic phase throughout the reaction.[42] We found that initial stirring of the catalyst precursors in a small amount of piperidine,[43] before addition of the remaining reagents, also improved the yield of 1,2-bis(4-methoxyphenyl)ethyne which was demethylated with BBr_3 to give H_2(**C≡C**).

H_2(**NN**) was prepared from 4-aminophenol by (i) protection of the phenol with an $^iPr_3Si$ group, (ii) oxidative dimerisation of the aniline group and (iii) deprotection of the phenol with fluoride. H_2($C_2ΦC_2$) was prepared *via* a Heck coupling of 4-vinylanisole (two equivalents) with 1,4-dibromobenzene, followed by demethylation. The ligand 4,4′-dihydroxybenzophenone (H_2**CO**) is commercially available.

A note on the characterisation is appropriate at this point. The protected ligand precursors are generally soluble, stable species which have fully been characterised by the usual methods. The deprotected bis-phenol ligands, especially the longer ones, tend to be poorly soluble and not amenable to *e.g.* chromatographic purification. For this reason they were usually used crude as isolated from the deprotection reaction, as we found it much easier to purify the stable, soluble metal complexes by chromatography and recrystallisation.

Syntheses of complexes; crystal structures of Mo_2(CO) and Mo_2(NN)

All of the dinuclear complexes were prepared by the same general route that we have described before, *viz.* reaction of $[Mo^V(Tp^{Me,Me})(O)Cl_2]$ (>2 equivalents) with the deprotonated (using Et_3N) bridging ligand in toluene at reflux. Purification by column chromatography with silica/CH_2Cl_2 afforded pure products in all cases; salient characterisation data (FAB mass spectra and elemental analyses) are collected in Table 1. Solution EPR spectra of all of the complexes confirmed their formulation as dinuclear molybdenum(V) species, with g_{av} = 1.94 and a hyperfine pattern consistent with coupling of both unpaired electrons to both molybdenum centres (*i.e.* overlapping singlet, sextet and undecet components with a separation of *ca.* 25 Gauss between adjacent hyperfine signals). Such spectra are entirely characteristic of dinuclear oxo-molybdenum(V) complexes in which the two unpaired electrons are exchange-coupled, as discussed in detail earlier.[1,8]

Two of the complexes, **Mo_2(CO)** and **Mo_2(NN)**, afforded X-ray quality crystals and the structures are shown in Fig. 1 (see also Tables 2 and 3). In both cases the coordination geometry around the molybdenum(V) centres is unremarkable; both structures show the common[3,5,6,8] disorder between the oxo and chloride ligands which renders Mo=O and Mo–Cl distances inaccurate. The important point in each structure is the influence of the bridging ligand. In **Mo_2(CO)** the bridging benzophenone unit is buckled with an angle of 52° between the mean planes of the two aromatic rings. This type of conformation is typical of benzophenone units in the solid state.[44–48] In contrast, in the structure of **Mo_2(NN)** the bridging ligand is planar, as required by the crystallographic inversion centre at the centre of the N=N linkage. The intermolecular Mo···Mo separations are 11.87 and 14.61 Å respectively.

Electrochemical properties

(i) General considerations. The redox properties of the complexes were examined by cyclic and square-wave voltammetry, and the results are collected in Table 4. The general pattern that we have observed in our earlier studies has been preserved, *viz.* that the complexes generally show two clearly separated one-electron processes [previously assigned as Mo(VI)–Mo(V) couples] at positive potentials, and a single larger wave [corresponding to two coincident Mo(V)–Mo(IV) couples] at an approximately invariant negative potential (Fig. 2).[2,3,8] The fact that the oxidations are separated but the reductions are coincident, *i.e.* the oxidised mixed-valence state has a much higher comproportionation constant than the reduced mixed-valence state, has been ascribed to the fact that bridging bis-phenolate ligands of this type are themselves oxidisable to give semiquinones and then quinones, whereas they are not reducible.

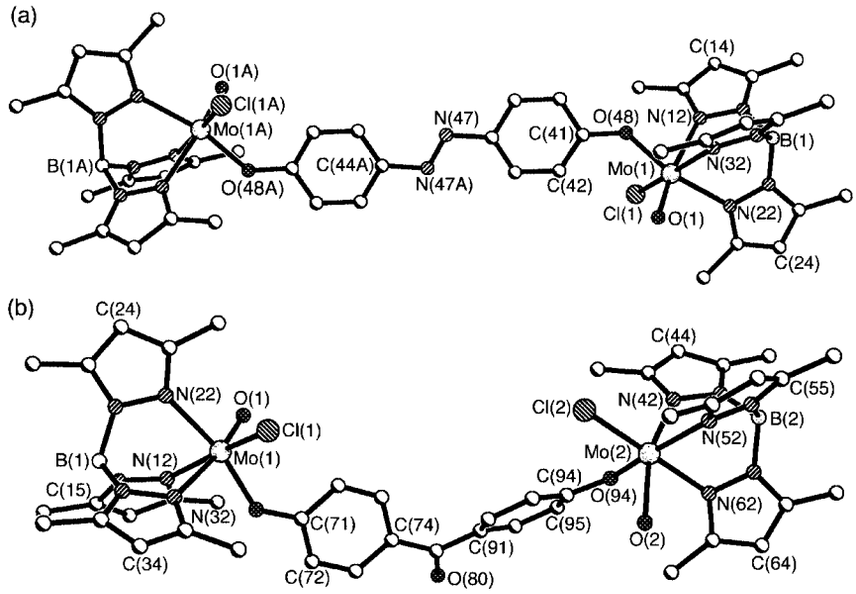

Fig. 1 Crystal structures of the dinuclear complexes (a) **Mo_2(NN)** and (b) **Mo_2(CO)**.

Table 2 Selected bond distances (Å) and angles (°) for **Mo_2(CO)**·$0.5C_5H_{12}$·$1.5CH_2Cl_2$ [a]

Mo(1)–O(1′)	1.72(2)	Mo(2)–O(2′)	1.727(14)
Mo(1)–O(1)	1.76(2)	Mo(2)–O(2)	1.742(13)
Mo(1)–O(71)	1.952(5)	Mo(2)–O(94)	1.924(5)
Mo(1)–N(22)	2.180(7)	Mo(2)–Cl(2′)	2.197(7)
Mo(1)–N(12)	2.213(6)	Mo(2)–N(52)	2.169(7)
Mo(1)–N(32)	2.223(6)	Mo(2)–N(62)	2.224(6)
Mo(1)–Cl(1)	2.318(8)	Mo(2)–N(42)	2.235(7)
Mo(1)–Cl(1′)	2.325(9)	Mo(2)–Cl(2)	2.287(7)
O(1′)–Mo(1)–O(71)	100.0(9)	O(2′)–Mo(2)–O(94)	99.3(5)
O(1)–Mo(1)–O(71)	98.5(7)	O(2)–Mo(2)–O(94)	98.3(8)
O(1′)–Mo(1)–N(22)	88.7(9)	O(2′)–Mo(2)–Cl(2′)	107.4(6)
O(1)–Mo(1)–N(22)	89.4(7)	O(94)–Mo(2)–Cl(2′)	95.5(3)
O(71)–Mo(1)–N(22)	167.2(2)	O(2′)–Mo(2)–N(52)	88.0(5)
O(1′)–Mo(1)–N(12)	168.6(8)	O(2)–Mo(2)–N(52)	91.0(8)
O(1)–Mo(1)–N(12)	90.9(7)	O(94)–Mo(2)–N(52)	165.6(3)
O(71)–Mo(1)–N(12)	85.8(2)	Cl(2′)–Mo(2)–N(52)	94.1(3)
N(22)–Mo(1)–N(12)	84.0(2)	O(2′)–Mo(2)–N(62)	163.3(6)
O(1′)–Mo(1)–N(32)	90.8(9)	O(2)–Mo(2)–N(62)	86.3(7)
O(1)–Mo(1)–N(32)	168.8(8)	O(94)–Mo(2)–N(62)	85.7(2)
O(71)–Mo(1)–N(32)	86.9(2)	Cl(2′)–Mo(2)–N(62)	87.9(3)
N(22)–Mo(1)–N(32)	83.7(2)	N(52)–Mo(2)–N(62)	83.9(3)
N(12)–Mo(1)–N(32)	79.7(2)	O(2′)–Mo(2)–N(42)	83.9(6)
O(1)–Mo(1)–Cl(1)	102.1(7)	O(2)–Mo(2)–N(42)	165.6(7)
O(71)–Mo(1)–Cl(1)	95.0(3)	O(94)–Mo(2)–N(42)	86.3(3)
N(22)–Mo(1)–Cl(1)	93.1(3)	Cl(2′)–Mo(2)–N(42)	168.0(3)
N(12)–Mo(1)–Cl(1)	166.8(3)	N(52)–Mo(2)–N(42)	82.1(3)
N(32)–Mo(1)–Cl(1)	87.2(3)	N(62)–Mo(2)–N(42)	80.4(2)
O(1′)–Mo(1)–Cl(1′)	98.7(9)	O(2)–Mo(2)–Cl(2)	94.2(7)
O(71)–Mo(1)–Cl(1′)	94.0(4)	O(94)–Mo(2)–Cl(2)	94.5(2)
N(22)–Mo(1)–Cl(1′)	93.9(4)	N(52)–Mo(2)–Cl(2)	95.8(2)
N(12)–Mo(1)–Cl(1′)	90.6(4)	N(62)–Mo(2)–Cl(2)	179.4(2)
N(32)–Mo(1)–Cl(1′)	170.1(4)	N(42)–Mo(2)–Cl(2)	99.0(2)

[a] The oxo and chloride ligands at each Mo are independently disordered. The site occupancies are as follows: O(1) and Cl(1), 0.52; O(1′) and Cl(1′), 0.48; O(2) and Cl(2), 0.45; O(2′) and Cl(2′), 0.55. Owing to this disorder, distances and angles involving these atoms will be relatively inaccurate.

Thus, delocalisation of the oxidised mixed-valence state occurs *via* hole transfer through the bridging ligand HOMO because the states Mo^{VI}–(L^{2-})–Mo^{V} and Mo^{V}–(L^{-})–Mo^{V} are not very different in energy.[3,8] In contrast, reduction of the dianionic bridging ligand is difficult, so delocalisation of the extra electron in the reduced mixed-valence state *via* the bridging-ligand LUMO [Mo^{IV}–(L^{2-})–Mo^{V} ⟶ Mo^{V}–(L^{3-})–Mo^{V}] is not feasible.

Table 3 Selected bond distances (Å) and angles (°) for **Mo_2(NN)** [a]

Mo(1)–O(1′)	1.782(13)	Mo(1)–Cl(1′)	2.216(6)
Mo(1)–O(1)	1.792(19)	Mo(1)–N(32)	2.221(5)
Mo(1)–O(48)	1.945(4)	Mo(1)–Cl(1)	2.226(6)
Mo(1)–N(22)	2.172(5)	Mo(1)–N(12)	2.230(5)
O(1′)–Mo(1)–O(48)	99.9(5)	Cl(1′)–Mo(1)–N(32)	94.0(2)
O(1)–Mo(1)–O(48)	98.3(7)	O(1)–Mo(1)–Cl(1)	100.2(6)
O(1′)–Mo(1)–N(22)	88.2(5)	O(48)–Mo(1)–Cl(1)	94.5(2)
O(1)–Mo(1)–N(22)	89.5(7)	N(22)–Mo(1)–Cl(1)	95.0(2)
O(48)–Mo(1)–N(22)	166.50(15)	N(32)–Mo(1)–Cl(1)	173.9(2)
O(1′)–Mo(1)–Cl(1′)	99.6(5)	O(1′)–Mo(1)–N(12)	86.9(5)
O(48)–Mo(1)–Cl(1′)	93.9(2)	O(1)–Mo(1)–N(12)	164.3(6)
N(22)–Mo(1)–Cl(1′)	95.4(2)	O(48)–Mo(1)–N(12)	85.03(17)
O(1′)–Mo(1)–N(32)	164.0(4)	N(22)–Mo(1)–N(12)	84.59(18)
O(1)–Mo(1)–N(32)	85.3(6)	Cl(1′)–Mo(1)–N(12)	173.5(2)
O(48)–Mo(1)–N(32)	87.45(16)	N(32)–Mo(1)–N(12)	79.55(18)
N(22)–Mo(1)–N(32)	82.19(17)	Cl(1)–Mo(1)–N(12)	94.8(2)

[a] The oxo and chloride ligands at the Mo are disordered. The site occupancies are as follows: O(1) and Cl(1), 0.46; O(1′) and Cl(1′), 0.54. Owing to this disorder, distances and angles involving these atoms will be relatively inaccurate.

Table 4 Electrochemical and magnetic data for the complexes

	Redox potentials, V *vs.* Fc–Fc^+				
Complex	Mo(v)–Mo(iv) [a]	**A** [b]	**B** [b]	$\Delta E_{1/2}$/mV	J/cm^{-1}
Mo_2(th)	−1.15	+0.33 [c]	+0.70 [c]	370	−3.6
Mo_2(th)$_2$	−1.11	+0.44 [c]	+0.69 [d]	250	0
Mo_2(th)$_3$ [e]	−1.12	+0.34 [c]	+0.51 [d]	170	[f]
Mo_2(C=C)	−1.18	+0.35 [c]	+0.69 [c]	340	−11.2
Mo_2(C=C)$_2$	−1.16	+0.28 [c]	+0.48 [d]	200	[f]
Mo_2(C=C)$_3$	−1.20	+0.26 [c]	+0.38 [d]	120	[f]
Mo_2(C≡C)	−1.15	+0.53 [c]	+0.88 [d]	350	−7
Mo_2(N=N)	−1.13	+0.60 [c]	+0.82 [c]	220	−12.8
Mo_2(CO)	−1.07	+0.78 [c]	+0.91 [c]	130	−1.1
Mo_2($C_2ΦC_2$)	−1.15	+0.43 [c]	+0.56 [c]	130	[f]

[a] Two coincident, unresolved one-electron processes; peak–peak separation ΔE_p typically 100–150 mV. [b] See main text for definition of the couples **A** and **B**. [c] Reversible one-electron process: peak–peak separation in the range 70–100 mV, equal cathodic and anodic peak currents, and shown to be chemically reversible by spectroelectrochemistry. [d] Irreversible process: return wave of lower intensity than outward wave, and results in partial or total decomposition in the spectroelectrochemistry experiment. [e] A third oxidation is present for this compound, at +0.98 V *vs.* Fc–Fc^+, which appears to be reversible by cyclic voltammetry (see main text). [f] Not measured.

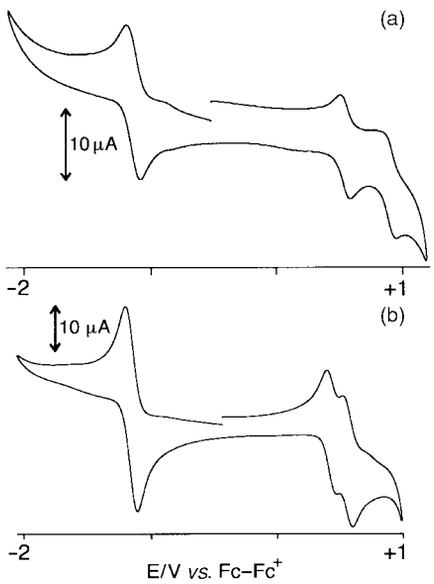

Fig. 2 Cyclic voltammograms of (a) $\mathbf{Mo_2(C{\equiv}C)}$ and (b) $\mathbf{[Mo_2(C_2\Phi C_2)]}$ (CH_2Cl_2, platinum bead working electrode, scan rate 0.2 V s^{-1}).

The non-innocence of the bridging ligands is obviously related to the properties of the numerous ruthenium(II) complexes of *o*-dioxolenes studied by both us[49–54] and by Lever and co-workers[55–57] in which there is strong mixing between metal- and ligand-centred frontier orbitals such that assignment of redox processes as metal- or ligand-centred can be difficult. The two well separated oxidations, formally Mo(V) ⟶ Mo(VI) processes, can therefore have some ligand-centred character. Description of these processes as 'Mo(VI)–Mo(V) couples' may therefore not be entirely appropriate, and to avoid confusion in the following discussion the successive redox processes are simply denoted **A** and **B**. In contrast the Mo(V) ⟶ Mo(IV) reductions are metal-localised.

(ii) The series $\mathbf{Mo_2(C{=}C)_n}$ and $\mathbf{Mo_2(th)_n}$ (n = 1, 2, 3). Starting with the series $\mathbf{Mo_2(C{=}C)_n}$ (n = 1, 2, 3) we see that the separation (ΔE) between redox processes **A** and **B** starts at a high value (340 mV) for n = 1, and steadily diminishes to 200 mV for n = 2 and 120 mV for n = 3. The decay in ΔE is clearly not linear: the *fractional* decrease in ΔE is about constant for each increase in n, and we can accordingly derive an 'attenuation coefficient' of about 0.59 for the C=C unit, which is the amount by which ΔE is multiplied as each additional C=C unit is inserted into the bridging ligand. For the complex with no double bonds in the pathway, *i.e.* the biphenyl-bridged complex $\mathbf{[Mo{-}O(C_6H_4)_2O{-}Mo]}$, ΔE is 480 mV. Simply extrapolating from the $\mathbf{Mo_2(C{=}C)_n}$ (n = 1–3) series, whose bridging ligands are approximately planar, would suggest a value of *ca.* 580 mV for this redox separation; however this does not take into account the twisted conformation of the biphenyl spacer which will decrease the interaction. The steady attenuation in ΔE as the number of ethenyl units increases is equally consistent with **A** and **B** being metal-centred or ligand-centred processes. Although both waves look symmetric on the timescale of cyclic voltammetry, spectroelectrochemical measurements (see later) showed that the second oxidation process (**B**) became more irreversible as more ethenyl units are added to the bridge.

For the series $\mathbf{Mo_2(th)_n}$ (n = 1, 2, 3) we again see substantial separations between redox couples **A** and **B**, with ΔE = 370, 250 and 170 mV respectively, giving a consistent attenuation coefficient of 0.68. For n = 1 both oxidations appear to be fully chemically reversible; for n = 2 and 3, the second oxidation is not fully reversible with the return wave of lower intensity than the outward wave (reasons for this are discussed later). For $\mathbf{Mo_2(th)_3}$ only, an additional third redox process appears at +0.98 V *vs.* $Fc{-}Fc^+$. The appearance of an extra redox process for this compound is consistent with the fact that oligothienyl fragments become easier to oxidise as they become longer,[58–61] so the appearance of an additional ligand-centred process is to be expected as more thienyl units are placed in the bridging ligand.

Each thienyl unit corresponds to two double bonds in the bridging pathway, yet each causes less of an attenuation in the electrochemical interaction than does a *single* ethenyl spacer (attenuation coefficient 0.59). These values may be compared with an average attenuation coefficient of 0.43 for the phenylene spacers in the series $\mathbf{[Mo{-}O(C_6H_4)_nO{-}Mo]}$ (n = 0, 1, 2). The attenuation coefficients reflect the ability of the different spacer groups to stabilise the mixed-valence complexes (whether metal- or ligand-based) by delocalisation of the odd electron. It is to be expected that thienyl units are more effective at this than phenylene units, for the reasons mentioned earlier: both spacers are about the same length, an additional two double bonds in the bridging pathway, but oligothienyl units are more coplanar than oligophenylene units.[27–30] It is surprising however that the thienyl spacer is also more effective than a single ethenyl unit at stabilising the mono-oxidised radicals by delocalisation, especially as polyene spacers are also expected to be approximately coplanar. The thienyl units are therefore acting as more than just planar butadienyl units. This must reflect the electronic contribution from the S atoms, whose π-symmetry orbitals will contribute to the delocalised orbital system of the bridging ligand. The result is that even across three thienyl spacers (crudely equivalent to six double bonds) the two redox couples are still significantly separated.

Previous studies on polyene-linked series of dinuclear complexes studied by Reimers and Hush,[12] and Launay, Spangler and co-workers[13] have shown an approximately exponential decrease in the electronic coupling parameter V_{ab} as the polyene chain lengthens; values of V_{ab} were determined from the properties of the inter-valence charge-transfer (IVCT) band for each compound. Our results, for both the ethenyl-spacer and thienyl-spacer series, are consistent with this general expectation. We have not been able to extract values of V_{ab} from the spectra of the Mo(VI)–Mo(V) complexes, because the expected IVCT transitions are obscured by much stronger LMCT transitions involving the molybdenum(VI) centre (*vide infra*). However as long as ΔE is dominated by the through-bond electronic coupling then it should show the same exponential decay with distance as does V_{ab},[13,14] as we observe.[62]

Apart from the separations between the two oxidation processes, their absolute values are also of interest. For the $\mathbf{Mo_2(C{=}C)_n}$ series the average of the two oxidation potentials shifts to less positive potential as the chain lengthens: 0.52 V *vs.* $Fc{-}Fc^+$ for n = 1; 0.38 V for n = 2; and 0.32 V for n = 3. If these two couples were totally metal-centred, we would say that this greater ease of oxidation reflected increased electron density at the metal centre. However this is not consistent with the fact that the redox potentials of the (metal-centred) Mo(V)–Mo(IV) couples are almost invariant across the series. This reduction of the redox potentials of couples **A** and **B** as the bridging ligand lengthens is however consistent with steadily increasing ligand-centred character for couples **A** and **B**. Similar behaviour, although not so clear-cut, was observed with the polyphenylene-bridged series of complexes $\mathbf{[Mo{-}O(C_6H_4)_n{-}O{-}Mo]}$ (n = 1–4).[8] The oligothienyl-bridged series $\mathbf{Mo_2(th)_n}$ does not show a clear trend at all, with the average potential for the two couples **A** and **B** being +0.52 (n = 1), +0.57 (2) and +0.43 V (3).

(iii) The dinuclear complexes $\mathbf{Mo_2(C{\equiv}C)}$, $\mathbf{Mo_2(N{=}N)}$, $\mathbf{Mo_2(CO)}$ and $\mathbf{Mo_2(C_2\Phi C_2)}$. For $\mathbf{Mo_2(C{\equiv}C)}$, the couples **A** and **B** are separated by 350 mV, the same as for $\mathbf{Mo_2(C{=}C)}$. In this case the alkynyl and alkenyl linkages are about equally as effective as each other at transmitting the electronic interaction. We[63,64] and others[65,66] have previously observed that alkynyl

spacers in other dinuclear complexes gave slightly smaller ΔE values than alkenyl spacers, although the differences were not large. The azo-linkage of **Mo_2(N=N)** however is a much less efficient conductor than an ethenyl linkage, with a ΔE value of only 220 mV. The highly twisted conformation of the bridging ligand in **Mo_2(CO)** accounts for the low ΔE value of 130 mV.

In contrast the ΔE value of 130 mV across the much longer bridging ligand of **$Mo_2(C_2\Phi C_2)$** is quite impressive given the distance involved, which is equivalent to four double bonds [*cf.* ΔE = 120 mV for **$Mo_2(C{=}C)_3$**]. It is much larger than would be expected if we just start from [**Mo**–O(C_6H_4)$_2$O–**Mo**] (ΔE = 480 mV) and apply the attenuation coefficients for each additional spacer in turn: with two double bonds and a phenylene unit this would suggest a ΔE value of about 480 × 0.59 × 0.59 × 0.43 = 72 mV. However, as mentioned above, pure oligophenylene chains are expected to be highly twisted and the attenuation effect of an additional phenylene spacer in these cases reflects not only the increased metal–metal separation, but also an additional twist to disrupt delocalisation in the bridging ligand. In **$Mo_2(C_2\Phi C_2)$** the phenylene spacer is necessarily coplanar with the rest of the bridging ligand, which results in it having a smaller attenuation effect than it does in the oligophenylene chains.

UV/VIS/NIR spectroelectrochemical behaviour (see Table 5)

(i) Properties of the phenylene-bridged complexes [Mo–O(C_6H_4)$_n$O–Mo]. Before discussing the spectroelectrochemical characteristics of the new complexes, it will be useful to summarise briefly the properties of the oligophenylene-bridged dinuclear complexes [**Mo**–O(C_6H_4)$_n$O–**Mo**] (n = 2, 3, 4) which we described in a previous paper.[3] In the Mo(V)–Mo(V) starting state the spectra of these show the typical features to be expected for the mononuclear model complex [Mo^V($Tp^{Me,Me}$)(O)Cl(OPh)], with the lowest-energy transition being a phenolate→Mo(V) LMCT in the region *ca.* 500–700 nm. On one-electron oxidation to the (formally) Mo(VI)–Mo(V) state, an intense near-IR transition appears (λ_{max} = 1096, 1131, 1047 nm for n = 2, 3, 4 respectively); on further oxidation to the (formally) Mo(VI)–Mo(VI) complex this transition is slightly blue-shifted (λ_{max} = 1017, 1015, 1033 nm respectively) and tends to be sharper and more intense than in the mixed-valence state (Fig. 3). In all three complexes the two one-electron oxidations are fully chemically reversible and the dication is indefinitely stable in solution under the conditions of the experiment.[3,8]

As mentioned above, the question arises as to the nature of the two oxidations as metal-based or ligand-based. The limiting canonical forms of the doubly oxidised species are depicted in Scheme 2. These can either be Mo(VI)–Mo(VI) complexes with a bis-phenolate bridge following metal-centred oxidation, or dinuclear molybdenum(V) complexes spanned by a bridging quinone following ligand-centred oxidation. The different electronic transitions expected for these extreme forms are included in Scheme 2. In particular, if the oxidations are metal-centred giving a Mo(VI)–Mo(V) and then a Mo(VI)–Mo(VI) complex, then intense, low-energy phenolate→Mo(VI) LMCT transitions are expected; if they are ligand-centred, we expect to see semiquinone-based and then quinone-based $\pi \longrightarrow \pi^*$ transitions of the bridging ligand (Scheme 2).[67–73] There is no doubt from a wealth of magnetic and EPR spectroscopic data that in the starting (neutral) state these complexes are Mo(V)–(μ-diphenolate)–Mo(V), with the highest-energy occupied orbitals being the singly occupied d_{xy} orbital on each metal, and the bridging ligand HOMO being below these.[1–3] On this basis we expect the first oxidation to be metal-centred; however it would only require a small change in the relative energies of

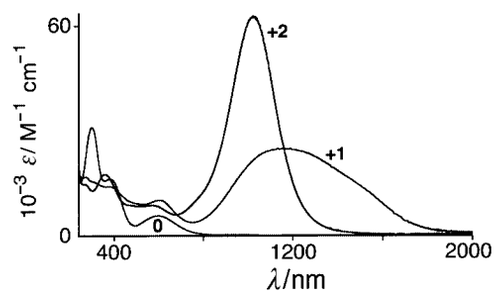

Fig. 3 Electronic spectra of [**Mo**–O(C_6H_4)$_3$O–**Mo**]$^{n+}$ (n = 0, 1, 2) (from ref. 3).

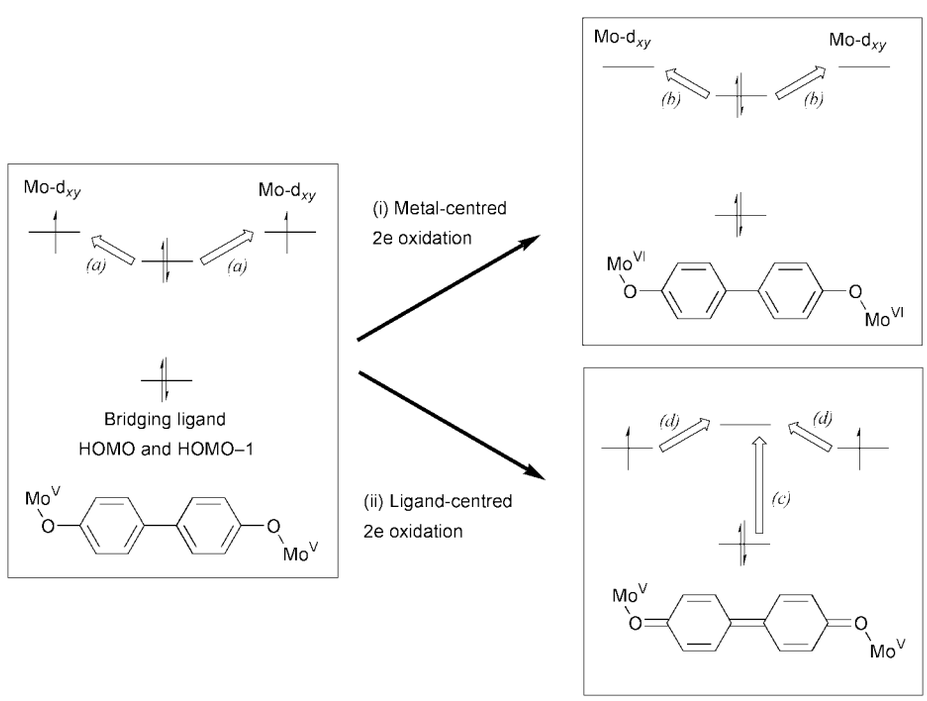

Scheme 2 Structures of the doubly oxidised forms of the dinuclear complexes arising from (i) purely metal-centred oxidations, and (ii) purely ligand-centred oxidations. The electronic transitions (hollow arrows) are: (a) phenolate→Mo(V) LMCT; (b) phenolate→Mo(VI) LMCT; (c) quinone-based $\pi \longrightarrow \pi^*$; and (d) Mo(V)→quinone($\pi^*$) MLCT.

ligand and metal frontier orbitals following the first oxidation to alter this picture for subsequent oxidations.

We concluded that the former description (metal-centred oxidations) was more appropriate in the series [**Mo**–O(C_6H_4)$_n$O–**Mo**], for several reasons. Firstly, ZINDO calculations supported the description of the near-IR transitions as phenolate→Mo(VI) LMCT processes in the doubly oxidised complexes. Secondly, the strong near-IR absorptions are characteristic of the low-energy phenolate→Mo(VI) LMCT process of mononuclear [Mo($Tp^{Me,Me}$)(O)Cl(OPh)]$^+$,[3] but are quite different from the spectra of the relevant free polyphenylene quinones whose $\pi \longrightarrow \pi^*$ transitions are much higher in energy.[67–73] Thirdly, the absorption maximum for the free quinone series becomes progressively red-shifted as the quinone lengthens,[69–73] which does not happen in the series [**Mo**–O(C_6H_4)$_n$O–**Mo**]$^{2+}$ (n = 2–4) where the near-IR absorption maximum hardly changes as the bridging ligand lengthens, consistent with phenolate→Mo(VI) LMCT character for the transitions. Fourthly, the observation that λ_{max} is similar in energy for both the mono- and di-oxidised forms (*e.g.* Fig. 3) is inconsistent with the behaviour of the free semiquinone and quinone species whose spectra are quite different;[67] it is however consistent with the presence of one and then two localised phenolate→Mo(VI) LMCT processes. These factors together strongly suggest two metal-centred oxidations for the series [**Mo**–O(C_6H_4)$_n$O–**Mo**].

(ii) Properties of the thienyl-bridged complexes Mo_2(th)$_n$. The electronic spectra of these complexes in the Mo(V)–Mo(V) state are generally similar to those of the other molybdenum(V) complexes discussed earlier, with the lowest-energy transition (630–660 nm) being a phenolate→Mo(V) LMCT and the higher-energy transitions having their usual assignments.[3,8]

One-electron oxidation of **Mo_2(th)** to the monocation [**Mo_2(th)**]$^+$ generates an intense new near-IR transition (λ_{max} = 1199 nm; ε = 56,000 M^{-1} cm^{-1}) which has a high-energy shoulder. The intensity and position of this are characteristic of a phenolate→Mo(VI) LMCT, as observed in the oligophenylene-bridged series,[3] and this is to be expected given that the HOMOs are the metal-based d_{xy} orbitals, each containing one electron (*cf.* EPR results, above; and magnetic susceptibility results, below). On further oxidation to [**Mo_2(th)**]$^{2+}$ this transition disappears and is replaced by one at much higher energy (684 nm) [Fig. 4(a)]. This behaviour is not consistent with a second metal-centred oxidation to give a Mo(VI)–Mo(VI) species, but is more consistent with oxidation of the bridging ligand to give a quinone (Scheme 2): the π–π* absorption maximum for the free quinone derived from **H_2th** is at 531 nm.[31] We suggest therefore that [**Mo_2(th)**]$^{2+}$ is more accurately described as [Mo(V)]$_2$(μ-quinone) than as [Mo(VI)]$_2$(μ-diolate). This requires that the second oxidation results in an internal redistribution of electrons such that the sequence of species formed after successive oxidations is Mo(V)(μ-diolate)Mo(V) $\longrightarrow$ Mo(V)(μ-diolate)Mo(VI) $\longrightarrow$ Mo(V)(μ-quinone)Mo(V), in marked contrast to the behaviour of the phenylene-spaced analogues (*cf.* Fig. 3); we return to this point later. The lower-energy transitions such as the shoulder at *ca.* 1000 nm could then have Mo(V)→quinone(π*) LMCT character.

Oxidation of [**Mo_2(th)$_2$**] to [**Mo_2(th)$_2$**]$^+$ likewise results in an intense near-IR transition (λ_{max} = 1342 nm; ε = 23,500 M^{-1} cm^{-1}) having a shoulder at the high-energy side [Fig. 4(b)], which we assign as a phenolate→Mo(VI) LMCT process following metal-centred oxidation. The particularly low energy of this redox-switchable transition makes it of interest for use in modulating near-IR lasers and we have recently described how this [**Mo_2(th)$_2$**]$^{0/+}$ couple can be exploited for near-IR optical switching.[26] Further oxidation to [**Mo_2(th)$_2$**]$^{2+}$ is however irreversible on the slow timescale of spectroelectrochemistry, with spectra showing clear evidence of decomposition of the dication. This irreversibility of the second oxidation is actually

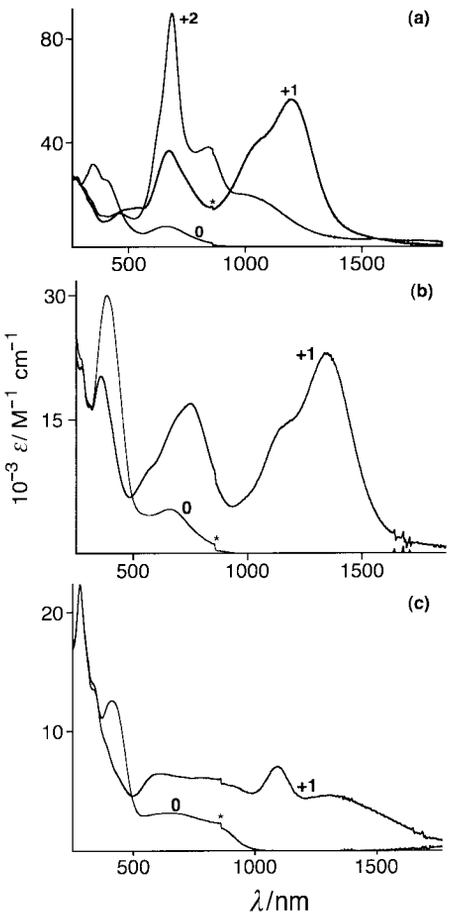

Fig. 4 Electronic spectra of (a) [**Mo_2(th)**]$^{n+}$ (n = 0, 1, 2); (b) [**Mo_2(th)$_2$**]$^{n+}$ (n = 0, 1); (c) [**Mo_2(th)$_3$**]$^{n+}$ (n = 0, 1) [* = detector change].

consistent with formation of a bridging quinone, for two reasons. Firstly, the electrostatic interaction between a neutral quinone O-donor and Mo(V) must be much weaker than between a negatively charged phenolate and Mo(VI). Others have observed how 2-electron oxidation of a coordinated aromatic diolate to a neutral quinone in a dinuclear complex results in its dissociation from the metal ions for this reason.[74] Secondly, extended quinones are known to be unstable because of the presence of a low-lying triplet excited state, in which unpaired electron density at C^2 and C^6 of the terminal rings (next to the oxygen atom) leads to oligomerisation. For this reason extended quinones such as *p*-terphenoquinone and *p*-quaterphenoquinone are prepared with bulky substituents to block these C^2 and C^6 positions which renders them much more stable.[71,73,75,76]

One-electron oxidation of [**Mo_2(th)$_3$**] to [**Mo_2(th)$_3$**]$^+$ again results in a broad region of absorbance in the near-IR region with two maxima resolved at 1304 and 1096 nm [Fig. 4(c)]. These are of rather low intensity compared to other such transitions in mono-oxidised complexes, but this is consistent with the substantial drop in intensity for the NIR transition between [**Mo_2(th)**]$^+$ and [**Mo_2(th)$_2$**]$^+$ and is possibly related to an increasing contribution from thienyl radical character, given the known ease of oxidation of oligothiophenes as they lengthen.[58–61] As we would expect by extrapolation from the properties of [**Mo_2(th)$_n$**] (n = 1, 2) the second oxidation is wholly irreversible on the spectroelectrochemistry timescale and clearly results in decomposition of the dication.

(iii) Properties of the ethenyl-bridged complexes Mo_2(C=C)$_n$. In all cases the spectra of the starting Mo(V)–Mo(V) states in this series are assignable as before.[3,8] For **Mo_2(C=C)**, oxidation to [**Mo_2(C=C)**]$^+$ results in the familiar phenolate→Mo(VI)

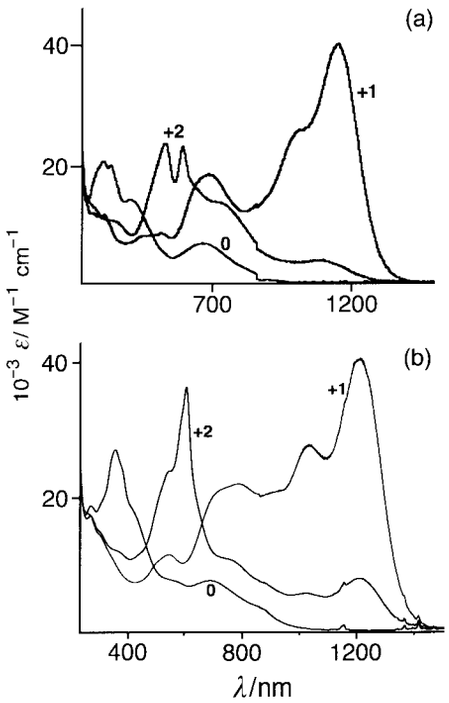

Fig. 5 Electronic spectra of (a) $[Mo_2(C{=}C)]^{n+}$ ($n = 0$, 1, 2); (b) $[Mo_2(C{=}C)_2]^{n+}$ ($n = 0$, 1, 2).

LMCT near-IR transition at 1151 nm ($\varepsilon = 40{,}000\ M^{-1}\ cm^{-1}$). Further oxidation to $[Mo_2(C{=}C)]^{2+}$ results in evolution of the spectra in a way similar to that seen on formation of $[Mo_2(th)]^{2+}$, *viz.* replacement of the NIR transition by a pair of transitions at much higher energy (500–600 nm), which is strongly characteristic of a quinone (for comparison, 3,3′,5,5′-tetra-*tert*-butyl-4,4′-stilbenequinone has $\lambda_{max} = 460$ nm)[67] but which is too high in energy to be a phenolate→Mo(VI) LMCT process [Fig. 5(a)]. As with $[Mo_2(th)]$ we are seeing spectroscopic behaviour indicative of a shift to ligand-centred oxidations following an internal charge redistribution associated with the second oxidation. Compared to [**Mo**–$O(C_6H_4)_2O$–**Mo**] (where both oxidations are metal-centred),[3] addition of the double bond between the two phenyl rings appears to have resulted in a greater degree of ligand-centred character for the oxidations, although this is not obviously reflected in the electrochemical properties of the respective free quinones.[67] In addition we note that the presence of two closely spaced absorption maxima in this case is in agreement with the electronic spectra of a variety of extended quinones.[67]

$Mo_2(C{=}C)_2$ behaves similarly, with the monocation giving a strong NIR phenolate→Mo(VI) LMCT transition ($\lambda_{max} = 1210$ nm; $\varepsilon = 41{,}000\ M^{-1}\ cm^{-1}$). The spectrum of the dication however shows a quinone-like absorption maximum at much higher energy (595 nm) [Fig. 5(b)], as we saw for $[Mo_2(C{=}C)]^{2+}$ and $[Mo_2(th)]^{2+}$. In keeping with our earlier observation that an increasing degree of quinone character in the doubly oxidised complex causes irreversibility of the second oxidation, we found that $[Mo_2(C{=}C)_2]^{2+}$ showed signs of decomposition: reduction back to **$Mo_2(C{=}C)_2$** regenerated the starting spectrum but with a loss of about 20% of its intensity after a few hours at −30 °C. For **$Mo_2(C{=}C)_3$** the problem was worse and only the monocation could be spectroscopically characterised ($\lambda_{max} = 1272$ nm; $\varepsilon = 21{,}000\ M^{-1}\ cm^{-1}$ for the NIR phenolate→Mo(VI) LMCT transition).

This series of complexes therefore behaves in a similar manner to $[Mo_2(th)_n]$ ($n = 1, 2$), in two respects. Firstly, oxidation **A** gives a NIR transition which is ascribable to a phenolate→Mo(VI) LMCT process following metal-centred oxidations, but oxidation **B** (when the product does not decompose) gives a spectrum characteristic of a bridging quinone which requires both oxidations to be ligand-centred. Secondly, as the ligand increases in length the doubly oxidised complex decreases in stability, which is also indicative of double ligand-centred oxidation as mentioned earlier.

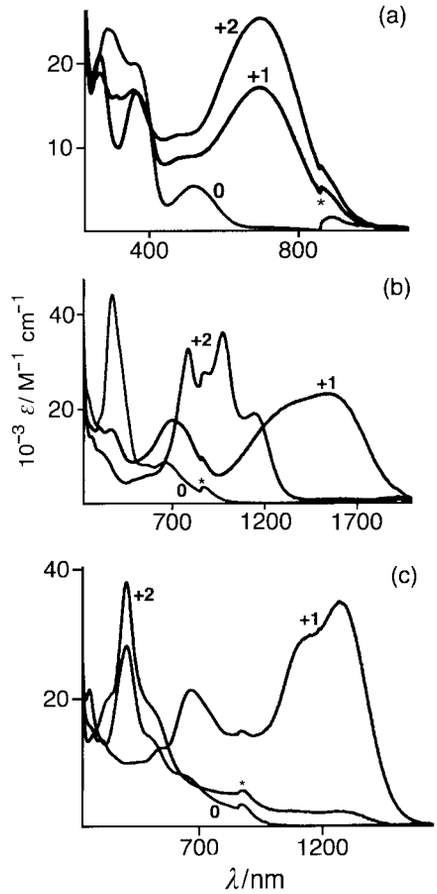

Fig. 6 Electronic spectra of (a) $[Mo_2(CO)]^{n+}$ ($n = 0$, 1, 2); (b) $[Mo_2(C_2\Phi C_2)]^{n+}$ ($n = 0$, 1, 2); (c) $[Mo_2(N{=}N)]^{n+}$ ($n = 0$, 1, 2) [* = detector change].

(iv) Properties of $Mo_2(C{\equiv}C)$, $Mo_2(N{=}N)$, $Mo_2(CO)$ and $Mo_2(C_2\Phi C_2)$. $Mo_2(CO)$ undergoes two successive metal-centred oxidations; in this case there is no ambiguity in the assignment as the bridging ligand cannot be oxidised to a quinone. The relatively high energy of the phenolate→Mo(VI) LMCT processes (695 and 698 nm for the mono- and di-cation respectively) [Fig. 6(a)] reflects the fact that the two termini are effectively decoupled by the twist in the ligand, such that each end behaves like an isolated molybdenum(VI) group, *cf.* the LMCT transition of $[Mo^{VI}(Tp^{Me,Me})(O)Cl(OPh)]^+$ at 681 nm.[3] In **$Mo_2(C{\equiv}C)$** the first oxidation is reversible and results in the typical NIR transition at 1052 nm, but the second oxidation is irreversible and results in decomposition.

The NIR transition arising from the first oxidation of **$Mo_2(C_2\Phi C_2)$**, at 1554 nm, is the longest-wavelength such transition we have seen so far and is in the region of the electromagnetic spectrum which is of particular interest for electro-optic switching [Fig. 6(b)].[26] On further oxidation to $[Mo_2(C_2\Phi C_2)]^{2+}$ there is a pronounced blue-shift of the new absorption maxima (1144 and 978 nm), which could be taken to indicate quinone formation, except that the shift is not as dramatic as would be expected: a ZINDO calculation suggests that the π–π* transition of the corresponding free quinone would be at 539 nm. It may be that the second oxidation in this case has more metal-centred character, which is consistent with the observation that both redox processes are fully chemically reversible.

In contrast, the azo-bridged complex **Mo_2(N=N)** shows most clearly of all those spectroscopic changes which we have ascribed to the shift from metal-centred to ligand-centred oxidation following the second redox process [Fig. 6(c)]. There is a dramatic difference between the principal absorption maxima for $[\mathbf{Mo_2(N{=}N)}]^+$ [λ_{max} = 1268 nm, characteristic of a phenolate→Mo(VI) LMCT process] and $[\mathbf{Mo_2(N{=}N)}]^{2+}$ (λ_{max} = 409 nm, indicative of quinone formation following the second oxidation). Although the corresponding free quinone is not known, a ZINDO calculation predicts its $\pi \longrightarrow \pi^*$ absorption maximum to be at 410 nm, in excellent agreement with our observations, and this behaviour is completely inconsistent with the occurrence of one and then two phenolate→Mo(VI) LMCT transitions following successive metal-centred oxidations (*cf.* the behaviour of the series [**Mo**–O(C_6H_4)$_n$O–**Mo**]).[3]

(v) Discussion of spectroelectrochemical results: metal-centred *vs*. ligand-centred redox activity. Starting with the monocations, as we mentioned earlier the obvious assignment for the NIR transition is a phenolate→Mo(VI) LMCT following metal-centred oxidation. This accords with the behaviour of the mononuclear molybdenum(VI) complex [Mo($Tp^{Me,Me}$)(O)Cl(OPh)]$^+$, and also the dinuclear complex series [**Mo**–O(C_6H_4)$_n$O–**Mo**]$^+$.[3] ZINDO calculations[77,78] on representative mono-oxidised complexes assuming a spin doublet state do a reasonable job of predicting an intense, low-energy LMCT transition in the NIR region between a bridging-ligand-based HOMO and a metal-based LUMO: for [**Mo**–O(C_6H_4)$_2$O–**Mo**]$^+$ we have λ_{max} (calculated) at 965 nm compared to an observed value of 1017 nm; for $[\mathbf{Mo_2(C{=}C)}]^+$ we have λ_{max} (calculated) at 1114 nm compared to an observed value of 1151 nm. The agreement is less good for $[\mathbf{Mo_2(N{=}N)}]^+$ for which λ_{max} (calculated) for the LMCT transition is at 883 nm, compared to an observed value of 1268 nm, and is even worse for $[\mathbf{Mo_2(C_2\Phi C_2)}]^+$ [λ_{max} (calculated) = 843 nm; observed, 1554 nm]. We note that the parameters used by ZINDO for second-row metals such as Mo are not as reliable as those for lighter elements, and that ZINDO is less accurate at predicting charge-transfer transitions than it is at predicting d–d and ligand-centred transitions.[77] Given these limitations, and the fact that the HOMOs of the neutral complexes are definitely the singly occupied metal-based d_{xy} orbitals, assignment of the first oxidation as formally metal-centred is straightforward.

For those dicationic complexes which were stable enough to be studied by spectroelectrochemistry, the intense transitions which we see in the UV and visible region are far more similar to the π–π* transition of the corresponding free quinones than they are to the phenolate→Mo(VI) LMCT processes which occur in the NIR region. As mentioned earlier, this requires an internal charge redistribution associated with the second oxidation, such that one-electron oxidation of Mo(V)(μ-diolate)-Mo(VI) affords Mo(V)(μ-quinone)Mo(V) (to the extent that such 'localised' descriptions are valid). There are several precedents for this in the literature, notably amongst first-row transition metal complexes with chelating *o*-dioxolenes of the type [catecholate]$^{2-}$ (cat) and [semiquinone]$^{\bullet -}$ (sq) from the work of Pierpont and co-workers. Thus, reversible one-electron reduction of [$Ni^{II}(sq)_2$] affords [$Ni^{III}(cat)_2]^-$, in which both ligands become reduced but the metal is oxidised,[79] and identical behaviour is shown by the [$Mn^{II}(sq)_2$]–[$Mn^{III}(cat)_2]^-$ couple.[80] A more dramatic charge redistribution occurs in [$V^{III}(sq)_3$], which on one-electron reduction affords [$V^{V}(cat)_3]^-$; a one-electron reduction of one sq ligand is accompanied by two-electron oxidation of the metal and one-electron reduction of each of the two remaining sq ligands.[81] Further examples of such redox rearrangements come from the work of Busch[82] and Wieghardt[83] and co-workers. Behaviour of this type may be ascribed to a change in the donor character of the ligand following a ligand-centred redox process, *e.g.* reducing a ligand will raise the energy of its frontier orbitals. If the metal- and ligand-based frontier orbitals are close in energy to start with, which is a defining characteristic of complexes containing non-innocent ligands, then this can result in an inversion of the order of the metal- and ligand-based electronic levels and an internal charge rearrangement. It is also worth mentioning other work from Pierpont and co-workers who have characterised numerous complexes showing 'valence tautomerism' in which *e.g.* Co^{II}(semiquinone) and Co^{III}(quinone) forms of the same complex (*i.e.* ligand-oxidised or metal-oxidised) are so close in energy that they can be interconverted by changes in temperature or pressure.[84–87] A more detailed analysis of the evolution of the electronic spectra of these complexes throughout the redox series will clearly require far more sophisticated methods such as *ab initio* or DFT calculations; these will be the subject of future work.

Table 5 UV/VIS/NIR Spectroelectrochemical data (CH_2Cl_2, −30 °C)

Complex	*n*	λ_{max}/nm (10^{-3} ε/M^{-1} cm^{-1})
$[\mathbf{Mo_2(th)}]^{n+}$	0	656 (7.9),[a] 414 (sh), 346 (31), 275 (26)
	1	1199 (56),[b] 673 (36.2), 275 (26.7)
	2	1000 (sh), 845 (37), 684 (87),[c] 456 (12), 276 (26)
$[\mathbf{Mo_2(th)_2}]^{n+}$	0	646 (5.2),[a] 381 (30), 270 (sh)
	1	1342 (24),[b] 752 (18), 359 (21), 269 (sh)
$[\mathbf{Mo_2(th)_3}]^{n+}$	0	636 (3.2),[a] 411 (13), 337 (sh), 281 (22)
	1	1304 (4.7), 1096 (7.1),[b] 612 (6.5), 337 (sh), 281 (22)
$[\mathbf{Mo_2(C{=}C)}]^{n+}$	0	666 (7.5),[a] 420 (18), 333 (26), 306 (27)
	1	1151 (40),[b] 1006 (sh), 692 (20), 500 (sh), 440 (10), 274 (16)
	2	1100 (4.6), 739 (sh), 594 (23),[c] 531 (24), 350 (sh)
$[\mathbf{Mo_2(C{=}C)_2}]^{n+}$	0	692 (7.8),[a] 357 (28), 274 (19)
	1	1210 (41),[b] 1038 (28), 787 (22), 545 (12), 267 (18)
$[\mathbf{Mo_2(C{=}C)_3}]^{n+}$	0	690 (sh),[a] 600 (10), 388 (37), 264 (23)
	1	1272 (21),[b] 1055 (18), 789 (18), 665 (32), 271 (23)
$[\mathbf{Mo_2(C{\equiv}C)}]^{n+}$	0	602 (5.1),[a] 376 (15), 285 (47)
	1	1052 (30),[b] 592 (29), 471 (13), 362 (14), 282 (23)
$[\mathbf{Mo_2(N{=}N)}]^{n+}$	0	644 (sh),[a] 505 (sh), 403 (27), 255 (22)
	1	1268 (35),[b] 1150 (sh), 672 (21), 557 (sh), 308 (14), 266 (sh)
	2	517 (sh), 409 (38),[c] 330 (sh)
$[\mathbf{Mo_2(CO)}]^{n+}$	0	523 (4.6),[a] 362 (sh), 287 (24.1)
	1	695 (12),[b] 513 (sh), 360 (sh), 274 (16)
	2	698 (20),[b] 487 (sh), 367 (14), 270 (17)
$[\mathbf{Mo_2(C_2\Phi C_2)}]^{n+}$	0	660 (6.3),[a] 550 (sh), 375 (44), 253 (sh)
	1	1554 (23),[b] 707 (18), 372 (16), 308 (16)
	2	1144 (20), 978 (37), 792 (33), 430 (sh), 266 (15)

[a] Phenolate→Mo(V) LMCT. [b] Phenolate→Mo(VI) LMCT (see main text). [c] Intense new transition in visible region for doubly oxidised complexes; tentatively ascribed to $\pi \longrightarrow \pi^*$ transition of bridging quinone (see main text).

Magnetic exchange interactions, and comparison with electrochemical interactions

The variable-temperature magnetic susceptibility behaviour of a selection of the complexes was measured with a SQUID magnetometer and the results are listed in Table 4. It will be seen that all complexes for which a value of *J* (the spin exchange coupling constant) could be determined are antiferromagnetically coupled. Comparison of the values for the different complexes shows some interesting effects.

Starting from [**Mo**–O(C_6H_4)$_2$O–**Mo**] for which $J = -13.2$ cm^{-1},[6] the interposed ethenyl spacer of **Mo_2(C=C)** has only a slight attenuating effect ($J = -11.2$ cm^{-1}). As with the electrochemical interaction, the increase in metal–metal separation will partly be offset by the more planar conformation of the bridge which is important for facilitating the exchange interaction.[6] The ethynyl spacer of **Mo_2(C≡C)** is significantly worse

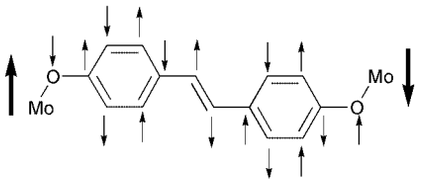

Fig. 7 Alternation of induced spins (small arrows) across the bridging ligand of **Mo_2(C=C)** resulting in antiferromagnetic exchange between the unpaired electrons on the metal centres (large arrows). A similar picture can be drawn for **Mo_2(NN)** and **Mo_2(C≡C)**.

at propagating the spin exchange interaction ($J = -7$ cm^{-1}), but interestingly the azo spacer of **Mo_2(N=N)** provides a stronger exchange interaction ($J = -12.8$ cm^{-1}) than the ethenyl spacer of **Mo_2(C=C)**, despite giving a weaker electrochemical interaction. The thienyl spacer of **Mo_2(th)** results in a weak exchange interaction ($J = -3.6$ cm^{-1}) despite being particularly effective at mediating electronic interactions. The twisted conformation of the bridging ligand in **Mo_2(CO)** results in poor spin exchange ($J = -1.1$ cm^{-1}) in agreement with its poor ability to mediate electrochemical interactions.

There is clearly not a good correlation between the ability of the different bridging ligands to mediate *electronic* interactions in the mixed-valence Mo(VI)–Mo(V) state (by delocalisation through a conjugated orbital system) and *magnetic* interaction in the isovalent Mo(V)–Mo(V) state (for which a spin-polarisation mechanism is valid in many cases).[2,4–7] The two types of interaction are presumably related to different properties of the bridging ligand. For those complexes of the type [**Mo**–O(C_6H_4)–X–(C_6H_4)O–**Mo**] for which we have both electrochemical and magnetic data, the effectiveness of spacer X at transmitting electronic interactions is **th** > (**C≡C** ≈ **C=C**) > **N=N** > **CO**; for magnetic interactions, the order is **N=N** > **C=C** > **C≡C** > **th** > **CO**. Apart from the poorest bridging ligand (dihydroxybenzophenone) which is fundamentally different from the others, both in its twisted conformation and the odd number of atoms in the bridge, the order of effectiveness for the four spacers **th**, **C≡C**, **C=C** and **N=N** is reversed.

We note that for **Mo_2(C=C)**, **Mo_2(N=N)** and **Mo_2(C≡C)** the presence of antiferromagnetic coupling is in agreement with our qualitative expectations on the basis of spin polarisation (Fig. 7).[2,5–7] The presence of an even number of atoms in the bridging pathway, whichever route is taken through the bridging ligand, means that the alternating pattern of induced spins will ensure that the unpaired electrons on the two **Mo** fragments will be spin-opposed in the ground state. For **Mo_2(th)** the situation is different because the thienyl ring contains an odd number of atoms: one pathway through the thienyl ring has four C atoms which would afford antiferromagnetic coupling on the basis of spin polarisation, whereas the other pathway has three atoms (C–S–C) which would give ferromagnetic coupling. It is tempting to speculate that the conflict between these two opposing effects means that they will tend to cancel one another out, an effect which has been suggested before in the context of electronic interactions,[88] which may partly explain why the **th** spacer is so poor at mediating magnetic exchange when it is so good at mediating electronic delocalisation. A more detailed study of magnetic exchange interactions across non-alternant bridging ligands of this type would be of interest.

We note also that for **Mo_2(CO)** the spin-polarisation picture fails: with a single additional atom in the pathway between the two phenyl rings, spin polarisation would predict ferromagnetic exchange. However we have found from earlier DFT calculations that other factors, such as the orientation of the **Mo** fragments with respect to the bridging ligand and to each other, also can make a significant contribution to the sign and magnitude of J.[4] These factors can over-ride spin-polarisation effects and this appears to be occurring with **Mo_2(CO)**.

Conclusions

Study of the redox, magnetic and spectroelectrochemical properties of dinuclear oxomolybdenum(V) complexes with bis-phenolate bridging ligands having a variety of spacers interposed between the phenyl rings has provided many insights into how the bridging ligands control the metal–metal electronic and magnetic interactions in the complexes. In particular we can draw the following conclusions.

(i) The efficiency of different types of spacer at providing delocalisation across the complex is thienyl > ethenyl > phenyl, with thienyl units being particularly effective at maintaining large redox separations ΔE over long distances. An ethenyl spacer is about as effective as an ethynyl spacer at mediating electronic interactions; the azo-spacer (N=N) is however significantly worse.

(ii) The oxidations of the complexes may be metal-centred or ligand-centred depending on how easily the bridging bis-phenolate bridging ligand can be oxidised to a quinone: the two types of dication have quite distinct electronic spectra. With oligophenylene bridges, spectroelectrochemical data (published earlier) indicate that both oxidations are metal-centred.[3] With a variety of other spacers such as ethenyl (1, 2 or 3), thienyl (1 or 2), the first oxidation again is largely metal-centred, but the second oxidation results in an electronic spectrum which is consistent with formation of [Mo(V)]$_2$(μ-quinone) species following internal charge redistribution associated with the second oxidation. In general, the doubly oxidised species whose electronic spectra are characteristic of a bridging quinone are unstable, which is consistent with dissociation of the poorly coordinating neutral quinone units and the known instability of extended quinones. In contrast metal-centred oxidations to give molybdenum(VI) phenolate species are fully reversible.

(iii) There is not a good correlation between the magnitudes of the electronic interactions and the magnetic interactions across different spacer units. In particular, thienyl units, which are the most effective at electronic delocalisation, are significantly worse than the other spacer units at mediating magnetic exchange.

(iv) The intense NIR transitions which appear in the oxidised forms of these complexes make them effective as electrochromic near-IR dyes in the region of the spectrum of interest for fibre-optic data transmission using silica fibres.

Experimental

General details

Instrumentation used for routine spectroscopic and electrochemical studies has been described recently.[89] Spectroelectrochemical studies were performed in CH_2Cl_2 solution at −30 °C using a home-built OTTLE (optically transparent thin-layer electrode) cell mounted in the sample compartment of a Perkin-Elmer Lambda 19 spectrophotometer as described previously;[89] the chemical reversibility of each process was checked by reversing the applied potential after electrolysis and ensuring that the spectrum of the starting material could be regenerated. Processes described as 'chemically reversible' fulfilled this criterion and also afforded isosbestic points in the overlaid spectra recorded during the redox conversion.

Magnetic susceptibilities were measured in the temperature range of 2–250 K in an applied field of 1 T using a Metronique Ingéniérie MS03 SQUID magnetometer; diamagnetic corrections were estimated from Pascal's constants.[90,91] The values of the parameters obtained by the fitting procedure using the exchange spin Hamiltonian $H = -J\ \boldsymbol{S}_1 \cdot \boldsymbol{S}_2$ (with positive J indicating ferromagnetism and negative J indicating antiferromagnetism) are included in Table 4.

[Mo($Tp^{Me,Me}$)(O)Cl_2] was prepared according to the method of Enemark and co-workers;[24] 2,5-bis(tri-n-butylstannyl)thio-

Table 6 Crystallographic data for the two structures[a]

	$Mo_2(CO)\cdot 0.5C_5H_{12}\cdot 1.5CH_2Cl_2$	$Mo_2(NN)$
Empirical formula	$C_{47}H_{61}B_2Cl_5Mo_2N_{12}O_5$	$C_{42}H_{52}B_2Cl_2Mo_2N_{14}O_4$
M	1264.8	1101.4
Crystal system, space group	Monoclinic, $C2/c$	Triclinic, $P\bar{1}$
a/Å	33.059(4)	11.060(5)
b/Å	19.737(4)	11.916(5)
c/Å	18.568(2)	11.985(6)
α/°		119.69(2)
β/°	98.070(9)	114.15(4)
γ/°		90.46(4)
V/Å^3	11996(3)	1206.9
Z	8	1
μ/mm^{-1}	0.692	0.687
Reflections collected: total/independent/R_{int}	31988, 10500, 0.0608	12455, 5481, 0.0899
Data/restraints/parameters	10500/78/747	5481/0/317
Final $R1$, $wR2$[b]	0.0746, 0.2493	0.0592, 0.1603

[a] Data in common: $T = 173$ K, $\lambda = 0.71073$ Å. [b] Structure was refined on F_o^2 using all data; the value of $R1$ is given for comparison with older refinements based on F_o with a typical threshold of $F \geq 4\sigma(F)$.

phene and 5,5″-bis(tri-n-butylstannyl)-2,2′:5′,2″-terthiophene were prepared according to the method of Miller and Yu.[92] The ligand H_2(**th**)$_2$ was available from previous work.[27] Organic starting materials were purchased from the usual commercial sources (Aldrich, Lancaster, Avocado) and used as received.

ZINDO calculations were carried out with INDO/1 parameters using the CAChe suite of programs on a Silicon Graphics Indy computer.[78] Structures were initially energy-minimised using the molecular mechanics method with MM3 parameters. The Mo–O–C–C dihedral angles were then set to 45° such that the plane of the phenolate ring bisected the Mo=O and Mo–Cl axes. This angle varies considerably in different crystal structures and we found that the results of the calculation are quite sensitive to this geometry as it affects the Mo[d(π)]–O[p(π)] overlap; accordingly we chose a representative geometry and fixed it for all of the molecules studied. For diamagnetic molecules the electronic spectra calculations (restricted Hartree–Fock, RHF) were performed with a configuration interaction level of 20; for paramagnetic species the electronic spectra calculations (restricted open-shell Hartree–Fock, ROHF) used a configuration interaction level of 18 which is the maximum allowed by the CAChe software.

X-Ray crystallography

Crystals of **$Mo_2(CO)$** and **$Mo_2(NN)$** were grown by diffusion of hexane into concentrated solutions of the complexes in CH_2Cl_2. In each case a suitable crystal was coated with hydrocarbon oil and attached to the tip of a glass fibre, which was then transferred to a Siemens SMART diffractometer under a stream of cold N_2 at 173 K. Details of the crystal parameters, data collection and refinement for each of the structures are collected in Table 6. After collection of a full sphere of data in each case an empirical absorption correction (SADABS) was applied,[93] and the structures were then solved by conventional direct methods and refined on all F^2 data using the SHELX suite of programs.[94] In all cases, non-hydrogen atoms were refined with anisotropic thermal parameters; hydrogen atoms were included in calculated positions and refined with isotropic thermal parameters which were *ca.* 1.2 × (aromatic CH) or 1.5 × (Me) the equivalent isotropic thermal parameters of their parent carbon atoms.

CCDC reference numbers 157071 and 157072.

See http://www.rsc.org/suppdata/dt/b1/b100681i/ for crystallographic data in CIF or other electronic format.

Syntheses of ligands

Me_2(C=C) [1,2-Bis(4-methoxyphenyl)ethene]. A mixture of 4-bromoanisole (2.0 g, 10.7 mmol), 4-methoxystyrene (1.87 g, 13.9 mmol), dry Et_3N (2 cm^3), $Pd(OAc)_2$ (0.048 g, 0.21 mmol) and PPh_3 (0.112 g, 0.428 mmol) in a sealed Schlenk tube under N_2 was heated to 100 °C for 3 days.[95] The resulting grey solid was partitioned between CH_2Cl_2 and water; the organic layer was separated, washed with water, and dried over $MgSO_4$. Removal of the solvent *in vacuo* afforded a crude green solid which was purified by column chromatography (alumina, CH_2Cl_2) to give 1,2-bis(4-methoxyphenyl)ethene [Me_2(**C=C**)] as a yellow solid in 58% yield. EIMS: *m*/*z* 240 (M^+). ^{1}H NMR (300 MHz, $CDCl_3$): δ 7.43 (4 H, d, $J = 8.8$; phenyl), 6.93 (2 H, s; vinylic CH), 6.89 (4 H, d, $J = 8.8$ Hz; phenyl), 3.83 (6 H, s; OCH_3). Found: C, 79.6; H, 7.1 (required for $C_{16}H_{16}O_2$: C, 80.0; H, 6.7%).

H_2(C=C) [1,2-Bis(4-hydroxyphenyl)ethene]. Demethylation of Me_2(**C=C**) was performed using BBr_3 in CH_2Cl_2 according to a published method.[31] After quenching the reaction mixture with water the product precipitated; the solid was filtered off, washed (water and CH_2Cl_2) and dried leaving H_2(**C=C**) as a red solid (45% yield). EIMS: *m*/*z* 212 (M^+). ^{1}H NMR (300 MHz, CD_3OD): δ 7.33 (4 H, d, $J = 8.6$; phenyl), 6.88 (2 H, s; vinylic CH), 6.75 (4 H, d, $J = 8.8$ Hz; phenyl).

$H_2(C{=}C)_2$ [1,4-Bis(4-hydroxyphenyl)butadiene]. The methylated precursor 1,4-bis(4-methoxyphenyl)butadiene [Me_2-(**C=C**)$_2$] was prepared from 4-methoxycinnamaldehyde and diethyl-4-methoxybenzylphosphonate according to a published procedure.[34] Demethylation of this to afford $H_2(C{=}C)_2$ was carried out using MeMgI as follows. To a solution of MeMgI [prepared under N_2 from Mg (0.3 g, 12 mmol) and MeI (0.75 cm^3, 1.71 g, 12 mmol) in Et_2O (20 cm^3)] was added with stirring a solution of $Me_2(C{=}C)_2$ (0.20 g, 0.75 mmol) in Et_2O (10 cm^3). The solvent was removed *in vacuo*, and the residue heated to 190 °C for 1 h. After cooling to room temperature, saturated aqueous NH_4Cl (50 cm^3) was added and the suspension further acidified by 1 M HCl. The solid which precipitated was extracted into Et_2O (4 × 50 cm^3), dried over $MgSO_4$, and the solvent evaporated to give $H_2(C{=}C)_2$ as a brown powder in 76% yield. EI-MS: *m*/*z* 238 (M^+). ^{1}H NMR (300 MHz, d^6-DMSO): δ 9.54 (2 H, broad; OH), 7.30 (4 H, d, $J = 8.6$; phenyl), 6.82 (2 H, dd, $J = 12.1$, 2.8; butadiene H^1/H^4), 6.74 (4 H, d, $J = 8.6$; phenyl), 6.54 (2H, dd, $J = 12.1$, 2.8 Hz; butadiene H^2/H^3).

$(PrOCH_2)_2(C{=}C)_3$ [1,6-Bis{4-(propoxymethoxy)phenyl}hexa-1,3,5-triene]. This follows a known method.[33] Freshly distilled glyme (1,2-dimethoxyethane) (50 cm^3) was slowly added under an argon atmosphere to a suspension of sodium hydride in glyme (80%, 3.75 g, 125 mmol). A mixture of freshly distilled 4-(propoxymethoxy)benzaldehyde (11.7 g, 60 mmol) and

1,4-but-2-enediylbis(diethyl phosphonate)[33] (9.90 g, 30 mmol) in glyme (25 cm^3) was added dropwise at room temperature. The reaction is exothermic during the initial addition. The reaction mixture was stirred at room temperature for 72 h and then heated under reflux for 2 h. After cooling, ^{i}PrOH (10 cm^3) was added to destroy unchanged NaH. The dark brown suspension was then poured onto ice–water (700 cm^3) to give a yellow flaky solid. After filtration and drying *in vacuo*, the crude product was dissolved in CH_2Cl_2, purified by flash chromatography (alumina, CH_2Cl_2) and recrystallised from methylcyclohexane. Yield: 35%. EIMS: *m*/*z* 408 (M^+). ^{1}H NMR (300 MHz, $CDCl_3$): δ 0.90 (6 H, t, J = 7.4; CH_3), 1.60 (4 H, m, $CH_3C\mathbf{H}_2$), 3.62 (4 H, t, J = 6.6; $CH_2C\mathbf{H}_2O$), 5.22 (4 H, s; $OC\mathbf{H}_2C_6H_4$), 6.50 (4 H, m; alkenyl), 6.75 (2 H, m; alkenyl), 6.99 (4 H, d, J = 8.7; phenyl), 7.33 (4 H, d, J = 8.7 Hz; phenyl). Found: C, 76.6; H, 7.4 (required for $C_{26}H_{32}O_4$: C, 76.5; H, 7.8%).

$H_2(C{=}C)_3$ [1,6-Bis(4-hydroxyphenyl)hexatriene]. To a stirred solution of $(PrOCH_2)_2(\mathbf{C}{=}\mathbf{C})_3$ (0.753 g, 1.9 mmol) in MeOH–thf (6 cm^3; 1 : 2, v/v) was added concentrated HCl (1 cm^3). The mixture was stirred overnight and then water was added, resulting in formation of a yellow precipitate which was collected by filtration, washed with further water, and dried. Recrystallisation from hot dmf–water afforded pure $H_2(\mathbf{C}{=}\mathbf{C})_3$ as a yellow crystalline powder in 89% yield. EIMS: *m*/*z* 264 (M^+). ^{1}H NMR (300 MHz, d^6-DMSO): δ 9.62 (2 H, broad; OH), 7.33 (4 H, d, J = 8.6; phenyl), 6.86–6.73 (6 H, m; four phenyl H and hexatriene H^2/H^5), 6.54 (2 H, d, J = 15.4; hexatriene H^1/H^6), 6.49 (2 H, dd, J = 7.0, 3.0 Hz; hexatriene H^3/H^4).

(^{i}Pr$_3$Si)$_2$(N=N) [4,4′-Bis(triisopropylsiloxy)azobenzene]. To an ice-cold solution of 4-aminophenol (2.55 g, 23.4 mmol) in dry thf (150 cm^3) under N_2 was added NaH (60% dispersion in mineral oil: 1.2 g, 30 mmol) which resulted in the solution becoming cloudy. Triisopropylsilyl chloride (4.51 g, 23.4 mmol) was added and the mixture stirred overnight at room temperature. Unchanged NaH was destroyed by addition of MeOH (10 cm^3); the solvents were removed *in vacuo* leaving a brown liquid which was partitioned between CH_2Cl_2 and water. The organic layer was separated, washed with water, and dried over $MgSO_4$. The resulting brown oil [crude 4-(triisopropylsiloxy)aniline] was dissolved in toluene (200 cm^3) and MnO_2 (8 g, a large excess) was added.[96] The mixture was stirred at room temperature overnight and became deep red. After removal of MnO_2 by filtration, evaporation of the solvent *in vacuo* left a dark red oil, which was purified by column chromatography (alumina, CH_2Cl_2) to give 4,4′-bis(triisopropylsiloxy)azobenzene as a dark orange oil which solidified on cooling (34% yield based on aminophenol). EIMS: *m*/*z* 526 (M^+). ^{1}H NMR (300 MHz, $CDCl_3$): δ 7.80 (4 H, d, J = 9.0; phenyl), 6.97 (4 H, d, J = 9.0 Hz; phenyl), 1.1–1.3 (42 H, m; ^{i}Pr$_3$Si). Found: C, 68.8; H, 9.6; N, 4.9 (required for $C_{30}H_{50}N_2O_2Si_2$: C, 68.4; H, 9.5; N, 5.3%).

H_2(N=N) (4,4′-Azophenol). To a solution of (^{i}Pr$_3$Si)$_2$(N=N) (0.81 g, 1.54 mmol) in dry thf (50 cm^3) was added an excess of tetra(*n*-butyl)ammonium fluoride under N_2 at room temperature. On addition of the fluoride the orange solution became dark brown, and after 20 minutes a yellow precipitate formed. The mixture was stirred for 30 minutes, after which time the yellow solid was filtered off, washed with thf, and dried. The crude material was purified by column chromatography (silica, 10 : 1 ethyl acetate–CH_2Cl_2) to afford pure 4,4′-azophenol in 43% yield. EIMS: *m*/*z* 214 (M^+). ^{1}H NMR (300 MHz, CD_3OD): δ 7.74 (4 H, d, J = 9.2; phenyl), 6.89 (4 H, d, J = 9.1 Hz; phenyl). Found: C, 67.1; H, 4.7; N, 13.0 (required for $C_{12}H_{10}N_2O_2$: C, 67.3; H, 4.7; N, 13.1%).

$Me_2(C_2\Phi C_2)$ {1,4-Bis[2-(4-methoxyphenyl)ethenyl]benzene}. A mixture of 1,4-dibromobenzene (1.42 g, 6.0 mmol), 4-methoxystyrene (2.25 g, 16.8 mmol), $Pd(OAc)_2$ (0.027 g, 0.12 mmol), PPh_3 (0.063 g, 0.24 mmol) and dry Et_3N (2.5 cm^3) in a sealed Schlenk tube under N_2 was heated to 100 °C for 3 days, affording a green solid.[68] This was suspended in water, which dissolved the $[Et_3NH]Br$ and inorganic salts, and filtered; the resulting grey solid was washed copiously with water and then with a small amount of CH_2Cl_2 to give nearly pure $Me_2(\mathbf{C_2\Phi C_2})$ in 32% yield. EIMS: *m*/*z* 342 (M^+). ^{1}H NMR (300 MHz, $CDCl_3$): δ 7.46 (4 H, d, J = 8.4 Hz; phenyl), 7.30 (4 H, m; phenyl), 7.10 (2 H, m; vinylic CH), 6.90 (6 H, m; 4 phenyl and 2 vinylic CH). Found: C, 84.2; H, 6.8 (required for $C_{24}H_{22}O_2$: C, 84.2; H, 6.4%).

$H_2(C_2\Phi C_2)$ {1,4-Bis[2-(4-hydroxyphenyl)ethenyl]benzene}. Demethylation of $Me_2(\mathbf{C_2\Phi C_2})$ was performed with BBr_3 in CH_2Cl_2 according to a published method.[31] After quenching the reaction by addition of water, a precipitate formed which was filtered off, washed with water and CH_2Cl_2, and dried to give $H_2(\mathbf{C_2\Phi C_2})$ as a grey solid in 50% yield. EIMS: *m*/*z* 314 (M^+). It is too insoluble in common solvents for NMR spectroscopy.

Me_2(C≡C) [1,2-Bis(4-methoxyphenyl)ethyne]. [^{t}Bu$_4$N][HSO_4] (0.115 g, 0.34 mmol) and KOH (0.673 g, 12 mmol) were ground up together and added under N_2 to a stirred mixture of CuI (0.190 g, 1.0 mmol), PPh_3 (0.393 g, 1.5 mmol), $PdCl_2(PPh_3)_2$ (0.197 g, 0.28 mmol) and piperidine (1 cm^3). To this was added a solution of 2-methyl-3-butyn-2-ol (0.9 cm^3, 0.78 g, 9.3 mmol) and 4-iodoanisole (3.93 g, 17 mmol) in benzene–thf (9 : 1, 70 cm^3), and the resultant mixture heated to 80 °C for 24 h. After cooling to room temperature, saturated aqueous NH_4Cl (150 cm^3) was added, and the mixture stirred for 1 h and then extracted with toluene (4 × 100 cm^3). The combined organic extracts were dried over $MgSO_4$, filtered, and the solvent was removed *in vacuo*. The crude product was dissolved in hexane and once more filtered and evaporated to dryness. Pure pale yellow 1,2-bis(4-methoxyphenyl)ethyne was produced by recrystallisation from hot ethanol (61% yield). EI-MS: *m*/*z* 238 (M^+). ^{1}H NMR (300 MHz, $CDCl_3$): δ 7.45 (4 H, d, J = 9.0; phenyl), 6.87 (4 H, d, J = 9.0 Hz; phenyl), 3.82 (6H, s, CH_3).

H_2(C≡C) [1,2-Bis(4-hydroxyphenyl)ethyne]. Demethylation of $Me_2(\mathbf{C}{\equiv}\mathbf{C})$ was performed with BBr_3 as follows. To a solution of $Me_2(\mathbf{C}{\equiv}\mathbf{C})$ (0.200 g, 0.84 mmol) in CH_2Cl_2 (5 cm^3) was added BBr_3 (1.0 M solution in CH_2Cl_2: 1.6 cm^3, 1.6 mmol). The deep purple solution so obtained was stirred for 24 h and then poured into ice–water (250 cm^3). The suspended solid which formed was extracted into Et_2O (3 × 150 cm^3); and then the combined organic fractions were re-extracted with aqueous NaOH (2 M, 2 × 150 cm^3). The basic solution was acidified by dropwise addition of concentrated HCl to pH 2, and then extracted a final time with Et_2O (3 × 150 cm^3). These organic fractions were then dried over $MgSO_4$ and the solvent was evaporated to produce a red-brown solid, which after recrystallisation from hot aqueous EtOH gave $H_2(\mathbf{C}{\equiv}\mathbf{C})$ in 53% yield. EI-MS: *m*/*z* 210 (M^+, 100%). ^{1}H NMR (300 MHz, CD_3OD): δ 7.29 (4 H, d, J = 8.8; phenyl), 6.75 (4 H, d, J = 8.8 Hz; phenyl).

Me_2th [2,5-Bis(4-methoxyphenyl)thiophene]. To a solution of 2,5-bis(tri-n-butylstannyl)thiophene (4.35 g, 6.6 mmol) in dry toluene (50 cm^3) under N_2 was added $Pd(PPh_3)_4$ (0.10 g, 87 μmol) and 4-bromoanisole (2.25 cm^3, 3.36 g, 18 mmol); the mixture was stirred at 100 °C for 24 h. The cooled mixture was poured into sat. aqueous NH_4Cl (100 cm^3) and the two phases were separated. The aqueous layer was further extracted with CH_2Cl_2 (3 × 100 cm^3), the combined organic extracts were dried over $MgSO_4$, and the solvent was evaporated to leave an oily yellow solid. The was dissolved in acetone and reprecipitated by addition of MeOH, leaving 2,5-di(4-methoxyphenyl)thiophene as a yellow-green powder in 26% yield. EIMS: *m*/*z* 296 (M^+). ^{1}H NMR (300 MHz, $CDCl_3$): δ 7.55 (4 H, dd, J = 6.8, 2.2; phenyl),

7.15 (2H, s; thienyl), 6.93 (4 H, dd, J = 6.6, 2.2 Hz; phenyl), 3.84 (6H, s; CH_3). Found: C, 72.6; H, 5.0 (required for $C_{18}H_{16}O_2S$: C, 73.0; H, 5.4%).

H_2th [2,5-Bis(4-hydroxyphenyl)thiophene]. Demethylation of Me_2**th** to give H_2**th** was accomplished with pyridine hydrochloride, as follows. Pyridine (technical grade, 10 cm^3) and conc. HCl (10 cm^3) were stirred together and heated to 200 °C in an open reaction flask under a stream of N_2. After *ca.* 1.5 h solid pyridinium chloride began to sublime around the neck of the flask. At this point Me_2**th** (0.20 g, 0.68 mmol) was added and the flask sealed. Heating and stirring were continued for 3 h. The reaction was allowed to cool and hot water (10 cm^3) added. The resultant mixture was poured into cold water (50 cm^3) and after cooling to room temperature the precipitate was collected by filtration. Recrystallisation of the crude material by addition of diethyl ether to an acetone solution of the solid afforded H_2**th** as a fluffy yellow solid (54% yield). EIMS: *m*/*z* 268 (M^+). ^{1}H NMR (300 MHz, d^6-acetone): δ 7.38 (4 H, dd, J = 6.6, 2.2; phenyl), 7.09 (2 H, s; thienyl), 6.76 (4 H, dd, J = 6.6, 2.2 Hz; phenyl).

Me_2(th)$_3$ [5,5″-Bis(4-methoxyphenyl)-2,2′:5′,2″-terthiophene]. To a solution of 5,5″-bis(tri-n-butylstannyl)-2,2′:5′,2″-terthiophene (1.96 g, 2.4 mmol) in dry toluene (25 cm^3) under N_2 was added $Pd(PPh_3)_4$ (65 mg, 56 μmol) and 4-bromoanisole (0.50 cm^3, 0.75 g, 4.0 mmol). The mixture was stirred and heated to 100 °C for 3 h. The cooled mixture was quenched by addition of water (40 cm^3) and the green-yellow precipitate collected by filtration. The filter-cake was slurried in thf (100 cm^3), filtered, and the residue extracted with further thf (700 cm^3). Evaporation of the solvent *in vacuo* left a brown residue which was washed with CH_2Cl_2 (100 cm^3) to leave 5,5″-bis(4-methoxyphenyl)-2,2′:5′,2″-terthiophene in 46% yield. EIMS: *m*/*z* 460 (M^+). Found: C, 67.2; H, 4.4 (required for $C_{26}H_{20}O_2S_3$: C, 67.8; H, 4.2%).

H_2(th)$_3$ [5,5″-Bis(4-hydroxyphenyl)-2,2′:5′,2″-terthiophene]. Demethylation of Me_2(**th**)$_3$ (0.20 g, 0.43 mmol) to give H_2(**th**)$_3$ was carried out with molten pyridinium chloride, exactly according to the method described above for H_2**th** except that the reaction temperature was maintained for 5 h. After cooling to below 100 °C, hot water (10 cm^3) was added and the mixture then poured into cold water (50 cm^3). The resulting suspension was saturated with NaCl and extracted with Et_2O–thf (3 : 1, 4 × 200 cm^3). The cloudy organic extracts were filtered, dried over $MgSO_4$, filtered once more, and evaporated to dryness to leave H_2(**th**)$_3$ as a green solid in 57% yield. EI-MS: *m*/*z* 432 (M^+).

Syntheses of complexes

All complexes were prepared by the same general method. A mixture of the bridging ligand (typically 0.3 mmol) and dry Et_3N (1 cm^3) in dry toluene under N_2 was heated to reflux for 15 minutes. After this time, [Mo(Tp^{Me,Me})(O)Cl_2] (0.7 mmol, slightly over two equivalents) was added and the mixture heated at reflux under N_2 until TLC analysis (silica, CH_2Cl_2) showed that no further change occurred. Typically this took 2 hours, but with the more insoluble bridging ligands such as H_2(**th**)$_3$ this could take up to 5 hours. After removal of the solvent *in vacuo*, the crude residue was purified by column chromatography on silica using CH_2Cl_2–hexane mixtures, varying from pure CH_2Cl_2 to 1 : 1 CH_2Cl_2–hexane according to how fast the principal fraction eluted. After collection of the main fraction and removal of solvents *in vacuo*, the complexes were purified by recrystallisation from CH_2Cl_2, by slow diffusion of either hexane or MeOH into the CH_2Cl_2 solution of the material.

Yields and characterisation data are collected in Table 1. All complexes were chromatographically pure by TLC analysis and gave correct molecular ions in their FAB mass spectra; elemental analyses were generally consistent with incorporation of some recrystallisation solvent, as detailed in the footnotes to Table 1. The sole exception to this was **Mo$_2$(C$_2$ΦC$_2$)** for which we could not obtain reliable analytical data; we have encountered this problem before with complexes of highly extended aromatic ligands.

Acknowledgements

We thank the European Community TMR Network programme (contract no. EC-CHRX-CT96-0047) and the EPSRC (UK) for financial support. M.D.W. is the Royal Society of Chemistry Sir Edward Frankland fellow for 2000/2001.

References

1 J. A. McCleverty and M. D. Ward, *Acc. Chem. Res.*, 1998, **36**, 3447.
2 S. Bayly, J. A. McCleverty, M. D. Ward, D. Gatteschi and F. Totti, *Inorg. Chem.*, 2000, **39**, 1288.
3 N. C. Harden, E. R. Humphrey, J. C. Jeffery, S.-M. Lee, M. Marcaccio, J. A. McCleverty, L. H. Rees and M. D. Ward, *J. Chem. Soc.*, *Dalton Trans.*, 1999, 2417.
4 A. Bencini, D. Gatteschi, F. Totti, D. N. Sanz, J. A. McCleverty and M. D. Ward, *J. Phys. Chem. A*, 1999, **102**, 10545.
5 V. A. Ung, S. M. Couchman, J. C. Jeffery, J. A. McCleverty, M. D. Ward, F. Totti and D. Gatteschi, *Inorg. Chem.*, 1999, **38**, 365.
6 V. A. Ung, A. M. W. Cargill Thompson, D. A. Bardwell, D. Gatteschi, J. C. Jeffery, J. A. McCleverty, F. Totti and M. D. Ward, *Inorg. Chem.*, 1997, **36**, 3447.
7 A. M. W. Cargill Thompson, D. Gatteschi, J. A. McCleverty, J. A. Navas, E. Rentschler and M. D. Ward, *Inorg. Chem.*, 1996, **35**, 2701.
8 V. A. Ung, D. A. Bardwell, J. C. Jeffery, J. P. Maher, J. A. McCleverty, M. D. Ward and A. Williamson, *Inorg. Chem.*, 1996, **35**, 5290.
9 A. Wlodarczyk, J. P. Maher, J. A. McCleverty and M. D. Ward, *J. Chem. Soc.*, *Dalton Trans.*, 1997, 3287.
10 M. D. Ward, *Chem. Soc. Rev.*, 1995, **24**, 121.
11 M. D. Ward, *Chem. Ind.*, 1996, 568.
12 J. R. Reimers and N. S. Hush, *Inorg. Chem.*, 1990, **29**, 3686.
13 A.-C. Ribou, J.-P. Launay, M. L. Sachtleben, H. Li and C. W. Spangler, *Inorg. Chem.*, 1996, **35**, 3735.
14 C. E. B. Evans, M. L. Naklicki, A. R. Revzani, C. A. White, V. V. Kondratiev and R. J. Crutchley, *J. Am. Chem. Soc.*, 1998, **120**, 13096.
15 F. Lloret, G. De Munno, M. Julve, J. Cano, R. Ruiz and A. Caneschi, *Angew. Chem.*, *Int. Ed.*, 1998, **37**, 135.
16 O. Kahn, *Molecular Magnetism*, VCH publishers, Inc., New York, 1993.
17 T. C. Brunold, D. R. Gamelin and E. I. Solomon, *J. Am. Chem. Soc.*, 2000, **122**, 8511.
18 S. Benard, P. Yu, J.-P. Audiere, E. Riviere, R. Clement, J. Guilhem, L. Tchernatov and K. Nakatani, *J. Am. Chem. Soc.*, 2000, **122**, 9444.
19 A. Escuer, J. Cano, M. A. S. Goher, Y. Journaux, F. Lloret, F. A. Mautner and R. Vicente, *Inorg. Chem.*, 2000, **39**, 4688.
20 C. Ruiz-Perez, M. Hernandez-Molina, P. Lorenzo-Luis, F. Lloret, J. Cano and M. Julve, *Inorg. Chem.*, 2000, **39**, 3845.
21 S. Triki, F. Berezovsky, J. S. Pala, E. Coronado, C. J. Gomez-Garcia, J. M. Clemente, A. Riou and P. Molinie, *Inorg. Chem.*, 2000, **39**, 3771.
22 Y. Cui, G. Chen, J. Ren, Y. T. Qian and J. S. Huang, *Inorg. Chem.*, 2000, **39**, 4165.
23 Q. D. Liu, S. Gao, J. R. Li, Q. Z. Zhon, K. B. Yu, B. Q. Ma, S. W. Zhang, X. X. Zhang and T. Z. Jin, *Inorg. Chem.*, 2000, **39**, 2488.
24 W. E. Cleland, Jr., K. M. Barhhart, K. Yamanouchi, D. Collison, F. E. Mabbs, R. B. Ortega and J. H. Enemark, *Inorg. Chem.*, 1987, **26**, 1017.
25 S.-M. Lee, M. Marcaccio, J. A. McCleverty and M. D. Ward, *Chem. Mater.*, 1998, **10**, 3272.
26 A. McDonagh, S. R. Bayly, D. J. Riley, M. D. Ward, J. A. McCleverty, M. A. Cowin, C. N. Morgan, R. Varrazza, R. V. Penty and I. H. White, *Chem. Mater.*, 2000, **12**, 2523.
27 J. Hock, A. M. W. Cargill Thompson, J. A. McCleverty and M. D. Ward, *J. Chem. Soc.*, *Dalton Trans.*, 1996, 4257.
28 A.-C. Ribou, J.-P. Launay, K. Takahashi, T. Nihira, S. Tarutani and C. W. Spangler, *Inorg. Chem.*, 1994, **33**, 1325.
29 P. Bäuerle, T. Fischer, B. Bidlingmeier, A. Stabel and J. P. Rabe, *Angew. Chem.*, *Int. Ed. Engl.*, 1995, **34**, 303.

30 J. Guay, A. Diaz, R. Wu and J. M. Tour, *J. Am. Chem. Soc.*, 1993, **115**, 1869.
31 K. Takahashi, T. Suzuki, K. Akiyama, Y. Ikegami and Y. Fukazawa, *J. Am. Chem. Soc.*, 1991, **113**, 4576.
32 W. H. Laarhoven, R. J. F. Nivard and E. Havinga, *Recl. Trav. Chim. Pays-Bas*, 1961, **80**, 775.
33 C. W. Spangler, R. K. McCoy, A. A. Dembek, L. S. Sapochak and B. D. Gates, *J. Chem. Soc.*, *Perkin Trans. 1*, 1989, 151.
34 K. Friedrich and W. Hartmann, *Chem. Ber.*, 1961, **94**, 840.
35 M. Takahasi, Y. Shioura, T. Murakami and K. Ogasawara, *Tetrahedron Asymmetry*, 1997, **8**, 1235.
36 M. Santelli and J.-M. Pons, *Lewis Acids and Selectivity in Organic Synthesis*, CRC press, Boca Raton, FL, 1996.
37 P. J. Kocienski, *Protecting Groups*, Georg Thieme, Stuttgart, 1994.
38 J. Trpin and B. G. Zupancic, *Monatsh. Chem.*, 1969, **100**, 114.
39 R. J. Kaufman and R. S. Sidhu, *J. Org. Chem.*, 1982, **47**, 4941.
40 K. Sonogashira, Y. Tohda and N. Hagihara, *Tetrahedron Lett.*, 1975, **50**, 4467.
41 D. E. Ames, D. Bull and C. Takundwa, *Synthesis*, 1981, 364.
42 C. Pugh and V. Percec, *Mol. Cryst. Liq. Cryst.*, 1990, **178**, 193.
43 M. Alami, F. Ferri and G. Linstrumelle, *Tetrahedron Lett.*, 1993, **34**, 6403.
44 P. K. A. Shonfield, A. Behrendt, J. C. Jeffery, J. P. Maher, J. A. McCleverty, E. Psillakis, M. D. Ward and C. Western, *J. Chem. Soc.*, *Dalton Trans.*, 1999, 4341.
45 H. M. Doesburg and J. H. Noordik, *Cryst. Struct. Commun.*, 1979, **8**, 377.
46 G. P. M. van der Velden and J. H. Noordik, *J. Cryst. Mol. Struct.*, 1980, **10**, 83.
47 G. M. Lobanova, *Kristallografiya*, 1968, **13**, 984.
48 M. More, G. Odou and J. Lefebvre, *Acta Crystallogr.*, *Sect. B*, 1987, **43**, 398.
49 L. F. Joulié, E. Schatz, M. D. Ward, F. Weber and L. J. Yellowlees, *J. Chem. Soc.*, *Dalton Trans.*, 1994, 799.
50 M. D. Ward, *Inorg. Chem.*, 1996, **35**, 1712.
51 A. M. Barthram, R. L. Cleary, J. C. Jeffery, S. M. Couchman and M. D. Ward, *Inorg. Chim. Acta*, 1998, **267**, 1.
52 A. M. Barthram, R. L. Cleary, R. Kowallick and M. D. Ward, *Chem. Commun.*, 1998, 2695.
53 A. M. Barthram and M. D. Ward, *New J. Chem.*, 2000, **24**, 501.
54 A. M. Barthram, Z. R. Reeves, J. C. Jeffery and M. D. Ward, *J. Chem. Soc.*, *Dalton Trans.*, 2000, 3162.
55 S. I. Gorelsky, E. S. Dodsworth, A. B. P. Lever and A. A. Vlcek, *Coord. Chem. Rev.*, 1998, **174**, 469.
56 A. B. P. Lever, H. Masui, R. A. Metcalfe, D. J. Stufkens, E. S. Dodsworth and P. R. Auburn, *Coord. Chem. Rev.*, 1993, **125**, 317.
57 R. S. da Silva, S. I. Gorelsky, E. S. Dodsworth, E. Tfouni and A. B. P. Lever, *J. Chem. Soc.*, *Dalton Trans.*, 2000, 4078.
58 J. Guay, A. Diaz, R. Wu and J. M. Tour, *J. Am. Chem. Soc.*, 1993, **115**, 1869.
59 J. Guay, P. Kasai, A. F. Diaz, R. Wu, J. M. Tour and L. H. Dao, *Chem. Mater.*, 1992, **4**, 1097.
60 M. G. Hill, J.-F. Penneau, B. Zinger, K. R. Mann and L. L. Miller, *Chem. Mater.*, 1992, **4**, 1106.
61 K. Takahashi and T. Suzuki, *J. Am. Chem. Soc.*, 1991, **111**, 5483.
62 This behaviour contrasts with a *linear* decrease in ΔE between two Mo(I)–Mo(0) couples across a bis(4-pyridyl)polyene ligand series, with up to 5 double bonds in the bridging pathway: J. A. Thomas, C. J. Jones, J. A. McCleverty, D. Collison, F. E. Mabbs, C. J. Harding and M. G. Hutchings, *J. Chem. Soc.*, *Chem. Commun.*, 1992, 1796.
63 A. J. Amoroso, A. M. W. Cargill Thompson, J. P. Maher, J. A. McCleverty and M. D. Ward, *Inorg. Chem.*, 1995, **34**, 4828.
64 A. Das, J. P. Maher, J. A. McCleverty, J. A. Navas Badiola and M. D. Ward, *J. Chem. Soc.*, *Dalton Trans.*, 1993, 681.
65 J. E. Sutton and H. Taube, *Inorg. Chem.*, 1981, **20**, 3125.
66 L. T. Cheng, W. Tam, S. H. Stevenson, G. R. Meredith, G. Rikken and S. R. Marder, *J. Phys. Chem.*, 1991, **95**, 10631.
67 J. Zhou and A. Rieker, *J. Chem. Soc.*, *Perkin Trans. 2*, 1997, 931.
68 K. Takahashi, A. Gunji, K. Yanagi and M. Miki, *J. Org. Chem.*, 1996, **61**, 4784.
69 W. J. Detroit and H. Hart, *J. Am. Chem. Soc.*, 1952, **74**, 5215.
70 O. B. Lantratova, A. I. Prokof'ev, I. V. Khudyakov, V. A. Kuzmin and I. F. Pokrovskaya, *Nouv. J. Chim.*, 1982, **6**, 365.
71 R. West, J. A. Jorgensen, K. L. Stearley and J. C. Calabrese, *J. Chem. Soc.*, *Chem. Commun.*, 1991, 1234.
72 P. Boldt, D. Bruhnke, F. Gerson, M. Scholz, P. G. Jones and F. Bär, *Helv. Chim. Acta*, 1993, **76**, 1739.
73 A. Rebmann, J. Zhou, P. Schuler, H. B. Stegmann and A. Rieker, *J. Chem. Res. (M)*, 1996, 1765.
74 M. Kurihara, I. Saito and Y. Matsuda, *Chem. Lett.*, 1996, 1109.
75 J. Bourdon and M. Calvin, *J. Org. Chem.*, 1957, **22**, 101.
76 K. Dimroth, W. Umbach and K. H. Blöcher, *Angew. Chem.*, *Int. Ed. Engl.*, 1963, **2**, 620.
77 See: http://btcpxx.che.uni-bayreuth.de/COMPUTER/Software/MSI/insight972/zindo/ZindoTOC.doc.html.
78 CAChe version 3.2, Oxford Scientific Ltd, Oxford, 1999.
79 C. W. Lange and C. G. Pierpont, *Inorg. Chim. Acta*, 1997, **263**, 219.
80 S. K. Larsen, C. G. Pierpont, G. De Munno and G. Dolcetti, *Inorg. Chem.*, 1986, **25**, 4828.
81 M. E. Cass, N. R. Gordon and C. G. Pierpont, *Inorg. Chem.*, 1986, **25**, 3962.
82 N. Takvoryan, K. Faramery, V. Katovic, F. V. Lovecchio, E. S. Gore, L. B. Anderson and D. H. Busch, *J. Am. Chem. Soc.*, 1974, **96**, 731.
83 B. de Bruin, E. Bill, E. Bothe, T. Weyhermüller and K. Wieghardt, *Inorg. Chem.*, 2000, **39**, 2936.
84 O. S. Jung, D. H. Jo, Y. A. Lee, Y. S. Sohn and C. G. Pierpont, *Inorg. Chem.*, 1998, **37**, 5875.
85 A. S. Attia and C. G. Pierpont, *Inorg. Chem.*, 1998, **37**, 3051.
86 O. S. Jung, D. H. Jo, Y. A. Lee, B. J. Conklin and C. G. Pierpont, *Inorg. Chem.*, 1997, **36**, 19.
87 O. S. Jung, D. H. Jo, Y. A. Lee, Y. S. Sohn and C. G. Pierpont, *Angew. Chem.*, *Int. Ed. Engl.*, 1996, **35**, 1694.
88 V. Marvaud, J.-P. Launay and C. Joachim, *Chem. Phys.*, 1993, **177**, 23.
89 S.-M. Lee, R. Kowallick, M. Marcaccio, J. A. McCleverty and M. D. Ward, *J. Chem. Soc.*, *Dalton Trans.*, 1998, 3443.
90 C. J. O'Connor, *Prog. Inorg. Chem.*, 1982, **29**, 203.
91 R. L. Carlin, *Magnetochemistry*, Springer Verlag, New York, 1986.
92 L. L. Miller and Y. Yu, *J. Org. Chem.*, 1995, **60**, 6813.
93 G. M. Sheldrick, SADABS, A program for absorption correction with the Siemens SMART area-detector system, University of Göttingen, 1996.
94 G. M. Sheldrick, SHELXS 97 and SHELXL 97, programs for crystal structure solution and refinement, University of Göttingen, 1997.
95 R. F. Heck, *Org. React.*, 1981, **27**, 345.
96 I. Bhatnagar and M. V. George, *J. Org. Chem.*, 1968, **33**, 2407.